Observation of Undertow and Turbulence in a Laboratory Surf Zone

by

Francis C. K. Ting and James T. Kirby

Research sponsored by
Office of Naval Research
Grant N00014-90-J168

RESEARCH REPORT NO. CACR-94-20
October, 1994

Center for Applied Coastal Research
Ocean Engineering Laboratory
University of Delaware
Newark, DE 19716

Observation of undertow and turbulence in a laboratory surf zone

Francis C. K. Ting [1], **James T. Kirby** [2]

[1] *Ocean Engineering Program, Department of Civil Engineering, Texas A&M University, College Station, TX 77843*

[2] *Center for Applied Coastal Research, Department of Civil Engineering, University of Delaware, Newark, DE 19716*

Abstract

Undertow and turbulence in the surf zone have been studied in a wave flume for a spilling breaker and a plunging breaker. Fluid velocities across a 1 on 35 sloped false bottom were measured using a fiber-optic laser-Doppler anemometer, and wave decay and set-up were measured using a capacitance wave gage. The characteristics of mean flow and turbulence in spilling versus plunging breakers were studied. The mean flow is the organized wave-induced flow defined as the phase average of the instantaneous velocity, while the turbulence is taken as the deviations from the phase average. It was found that under the plunging breaker turbulence levels are much higher and vertical variations of undertow and turbulence intensity are much smaller in comparison with the spilling breaker. It was also found that turbulent kinetic energy is transported seaward under the spilling breaker and landward under the plunging breaker by the mean flow. The study indicates that there are fundamental differences in the dynamics of turbulence between spilling and plunging breakers, which can be related to the processes of wave breaking and turbulence production. It is suggested that the types of beach profile produced by storm and swell waves may be the results of different relationships between mean flow and turbulence in these waves.

1. Introduction

It is well known that steep waves (e.g. storm waves) formed by a combination of large wave heights and short wave periods tend to result in seaward sediment transport and beach erosion, whereas milder and longer period waves (e.g. swell waves) move sediment onshore and produce an accretionary beach profile. Using a heuristic argument and small-scale laboratory data, Dean (1973) showed that the type of beach profiles can be predicted as a function of deep-water wave steepness and ratio of sediment fall velocity to wave period, that is

$$\frac{H_0}{L_0} = 1.7\frac{\pi}{g}\frac{w_f}{T} \tag{1}$$

where H_0 and L_0 are the deep-water wave height and wavelength, respectively, T is the wave period, w_f is the sediment fall velocity, and g is the gravitational acceleration. The heuristic model separates wave conditions into erosional and accretional regimes based on whether or not the value of H_0/L_0 exceeds the value given by Eq. 1. Similar formulae were developed by Kriebel et al. (1986), Kraus and Larson (1988), and Larson and Kraus (1989) using large-scale wave tank data. These results have been summarized recently by Dalrymple (1992), who showed that the separation of erosional and accretional wave conditions can be done concisely based on the value of a profile parameter, P, given by

$$P = \frac{gH_0^2}{w_f^3 T}. \tag{2}$$

Dalrymple showed that a value of P somewhere in the range of $9,000 < P < 10,500$ separates the two regimes, with small values of P indicating accretional conditions.

The heuristic model represents one of the major advances for classification of erosional and accretionary beach profiles. The model is based on consideration

of whether sediment suspended during wave breaking is acted upon predominantly by an onshore water particle velocity field or an offshore water particle velocity field as it falls to the bottom. Dean (1973) hypothesized that if the fall requires a short time relative to the wave period, then sediment will be acted on predominantly by onshore velocities. If, on the other hand, the fall time is long compared to the wave period, the predominant water particle velocity is directed offshore.

The heuristic model may be regarded as a statement about correlation between fluid velocity and suspended sediment concentration. It is known that suspension events make a significant contribution to sediment transport in the surf zone. Occurrence of such events have been observed in the field and in the laboratory by numerous investigators (e.g. Downing 1983, Jaffe et al. 1985, Beach and Sternberg 1988, Barkaszi and Dally 1993, Jaffe 1993). It was found that near-bottom sediment concentrations in the surf zone display a high degree of spatial and temporal variability. This is related to the variations with time and distance from the bed of the turbulence intensities. At the present time, it is believed that turbulent velocity fluctuations are responsible for keeping sediment in suspension, and the mean flow transports the sediment. Here, mean flow is defined as the ensemble average of the instantaneous velocity field over many repeated trials with identical test conditions, while deviations from the ensemble average are considered to be turbulence. Hence, mean flow is the organized wave-induced flow which includes both the undertow and the orbital wave motion. Because mean flow and turbulent velocity fluctuations vary with time, there would be an enhanced sediment transport during part of a flow oscillation; the rates and direction of sediment transport would depend on the relationship between mean flow and suspended sediment concentration. As velocity field and

sediment distribution are determined by incident wave conditions and sediment characteristics, it is not surprising that the heuristic model is able to discriminate between the two types of beach profile.

The results above provide the motivation for this study. The question which is the basis of this study is: what are the physical mechanisms that allow storm waves to carry sand offshore to form offshore bars, and swell waves to move sand onshore to produce an accretionary beach profile. If the beach slope is held fixed, the type of breakers would change from spilling to plunging as the wave steepness is decreased and the wave period is increased. Plunging breakers are characterized by a jet impinging on the oncoming trough and the subsequent violent transition from irrotational to rotational motion. Therefore, initial wave breaking in plunging breakers is fundamentally different from wave breaking in spilling breakers, the latter first appear as a broken water surface spilling down the front face of the wave. However, after a distance of several times the water depth at the breaking point, the broken wave has transformed into a turbulent bore. The height of the broken wave then remains an approximate fixed proportion of the mean water depth and the bores from a plunging breaker are visually similar to those originating from a spilling breaker (Svendsen et al., 1978). Nevertheless, in most situations there is a net offshore movement of sediment in spilling breakers and a net onshore movement in plunging breakers.

To investigate the flow conditions that produce erosional and accretionary profiles some comparisons are made in this paper between the velocity fields of a spilling breaker and a plunging breaker. Other investigators have presented velocity measurements in the surf zone. The present contribution focuses on the correlation between mean flow and turbulence. The important parameters that determine the type of breakers and the surf-zone dynamics are beach slope, wave

steepness and bottom roughness. In our experiments, the wave steepness H_0/L_0 of the plunging breaker was chosen to be much smaller than the wave steepness of the spilling breaker. For a typical sediment fall velocity, the spilling and plunging breakers could be classified as erosional and accretional waves, respectively. One of the remarkable results of our study is that though the turbulent bores from the spilling breaker are similar visually to those from the plunging breaker, their flow fields are substantially different. In particular, the temporal variation over a wave period of the turbulence intensity at a fixed point is small in the spilling breaker. This is consistent with a turbulence decay time that is large compared to the wave period. In contrast, we found that in the plunging breaker turbulence dies out between bores. Additionally, it was found that turbulent kinetic energy is transported seaward under the spilling breaker and landward under the plunging breaker by the mean flow. If it is assumed that turbulent velocity fluctuations are responsible for keeping sediment in suspension, and the mean flow transports the sediment, then suspended sediment transport superficially resembles turbulence transport, and there would be seaward sediment transport under the spilling breaker and landward sediment transport under the plunging breaker. It is suggested that the types of beach profile produced by storm and swell waves may be the result of different relationships between mean flow and turbulence in these waves. For that reason, predictive models of coastal processes must correctly model the spatial and temporal variations of turbulence in the surf zone and their relations to the mean flow to appropriately predict rates and direction of sediment transport.

2. Experimental equipment and procedures

The experiments were conducted in a two-dimensional wave tank in the

Ocean Engineering Laboratory at the University of Delaware. The wave tank is 40 m long, 0.6 m wide and 1.0 m deep. Waves were generated at one end of the tank by a bulkhead wave generator that was controlled by an electro-hydraulic servo-system. The system accepted an input voltage from an IBM PS/2 Model 30 286 computer; the displacement time history of the wave plate was proportional to the voltage time history of the input signal. A feedback system consisting of a linear variable differential transformer minimized the difference between the desired position of the wave plate and the actual position.

A schematic diagram of the experimental arrangement is shown in Fig. 1, where (x, z) is a Cartesian coordinate system with x measured positive shoreward from the toe of the slope and z extending positive upward from the undisturbed free surface. In this paper, ζ is the water surface elevation, $\overline{\zeta}$ is the mean water surface, H is the local wave height, d is the local still water depth, h is the local mean water depth, and the subscript b denotes the wave breaking point. A plywood false bottom was installed in the wave tank to create a uniform slope of 1 on 35. The still water depth in the constant-depth region of the wave tank was 0.4 m in all the experiments. The slope was sealed to the tank walls by inserting a polystyrene rod in between the edges of the slope and the side walls, and then filling the gap with silicone. Cnoidal waves were used in all the experiments. The control signal for the wave generator was computed using the numerical scheme by Goring (1978). Experiments were carried out for two different wave conditions; a spilling breaker of period 2.0 s and a plunging breaker of period 5.0 s. The wave heights in both cases were about 13 cm in the constant-depth region of the wave tank. Still water depths at breaking points of spilling and plunging breakers were 19.6 cm and 15.6 cm, respectively. Breaking points of spilling breakers are defined as the location where air bubbles begin to

be entrained in the wave crest, whereas those of plunging breakers are defined as the point where the front face of wave becomes nearly vertical.

Water surface elevations and velocities were measured at eight locations for the spilling breaker and seven locations for the plunging breaker along the centerline of the wave tank. Their exact locations are given in Table. 1. Velocity measurements were obtained using a two-component fiber-optic laser-Doppler anemometer (LDA) built by Dantec Electronics. The LDA was a backscatter, four-beam laser system. It consisted of a 100 mW air-cooled argon-ion laser, a transmitter, a 14 mm probe (focal length 50 mm, beam spacing 8 mm) and one frequency tracker and shifter for each velocity component. The Doppler frequency ranges used were 33 to 333 KHz for the spilling waves and 0.1 to 1 MHz for the plunging waves. The corresponding values of frequency shift used were 200 KHz and -500 KHz, respectively. It was found that the standard calibrations of the frequency trackers provided by Dantec Electronics have a non-negligible velocity offset that must be corrected. Therefore the frequency trackers were calibrated using a function generator and a frequency counter to obtain the analog representation of the detected Doppler frequency. After calibration the estimated error for the velocity measurements is ± 0.5 cm/s. Velocity measurements were obtained with the fiber-optic probe submerged. Unfortunately, the blue line of the laser did not have sufficient power therefore horizontal and vertical components of water-particle velocities were measured using the green line of the laser by conducting the same experiment twice. In the experiments, signal drop-out occurred when measuring above the level of the wave trough and in the bubble mass generated by wave breaking. Signal drop-out occurs when the tracker cannot follow the velocity changes in the turbulent flow. During signal drop-out the Doppler frequency is held at the last measured value. These events

were recorded by a built-in lock detector whose TTL (transistor-transistor logic) state in this case would change from HIGH to LOW. It was found that turbulence intensities were 5% to 10% higher if data obtained during signal drop-out were used, which therefore might not be interpreted as valid measurements. To miminize the influence of aeration on the velocity measurements, the lock detector signal was used to provide a first-level distinction between a valid Doppler signal and noise. Spikes in Doppler signals were observed when the probe volume of the LDA crossed the water surface resulting in spurious signals. In order to minimize signal bias, an additional validation procedure, based on checking the water level, was also used. A Doppler signal was considered valid if the measured water surface was above the probe and the lock detector signal was HIGH. When the probe was above the water surface the measured velocities were set equal to zero. Signals that did not meet either of these criteria were discarded.

Surface elevations were measured using capacitance wave gages. One wave gage and the fiber-optic probe were mounted on an instrument carriage which could slide along the top of the tank on two rails. A second wave gage was fixed at $x = -1.265\,\mathrm{m}$ to measure the incident wave amplitudes. It is noted that capacitance wave gage in principle cannot be used in aerated water. However, it was found that phase averages of water surface elevations in repeated trials were very near to being identical (see Fig. 8 and Fig. 17). Thus, the measurements may be regarded as representative of a water surface with an unknown void fraction.

Periodic waves were generated for a minimum of 20 minutes before data were taken. Hence, the measurements corresponded to a steady-state condition in the wave tank. Data were taken by an IBM PS/2 Model 30 286 computer installed

with a MetraByte DASH-16F data acquisition board. Sampling frequency was 100 Hz for each channel. Measurements consisted of time histories of wave plate motion, water surface elevations, Doppler and lock detector signals. Ensemble-averaged velocities were obtained by phase-averaging the measured signals separated by the wave period over one hundred and two successive waves; a signal which did not meet the validation criteria was not used in computing the phase average. The results, which represented the phase-averaged velocities at different phases of a wave cycle, were averaged to yield the time-mean velocities. The phase-averaged velocities were assumed to be the time-varying mean flow, and the turbulent velocity fluctuations were obtained by substracting the phase-averaged velocities from the original time series. The time-varying phase-averaged turbulent velocities over a wave cycle were computed by taking the square of the turbulent velocity fluctuations followed by phase-averaging and then computing the square root. Again, data that did not meet the validation criteria were not used in computing the phase-averaged turbulent velocities.

An attempt was made in our experiments to measure velocities above trough level. However, velocity measurements were made mainly below the trough level and above the bottom boundary layer. This is because data rate dropped sharply as the probe approached regions of relatively high concentration of air bubbles in the wave crest. The influence of aeration was more acute in the plunging breaker, which is to be expected. The variation of computed wave and turbulence statistics with the number of waves, N, are presented in Fig. 2 for the plunging breaker case. In this example, fluid velocities were measured at $(x - x_b)/h_b = 16.883$ and $(z - \overline{\zeta})/h = -0.456$; the trough level was located approximately at $(z - \overline{\zeta})/h = -0.4$. The total record, which consisted of one hundred and two waves, was divided into successively shorter records. A statistic, E_∞, computed

using the complete record, was taken as the "true" statistic, and a relative deviation was defined as

$$\Delta E = \frac{E_N - E_\infty}{E_\infty}. \tag{3}$$

Only data that met the validation criteria were used. Fig. 2 shows that the relative deviation is within $\pm 5\%$ when $N > 40$ for the time-mean horizontal velocity $\overline{u}$, the time-mean horizontal turbulent velocity $\overline{\sqrt{\widetilde{u'^2}}}$ and the time-mean vertical turbulent velocity $\overline{\sqrt{\widetilde{w'^2}}}$. The error associated with the time-mean vertical velocity $\overline{w}$ is larger because the current was small in the vertical direction. Since we have sampled one hundred and two waves there were enough realizations to provide stable wave and turbulence statistics though the highest point of measurement was made at 2.0 cm above the undisturbed water level.

The cross-shore transport of suspended sediment is influenced greatly by the correlation between organized wave-induced flow and suspended sediment concentration. Neglecting molecular diffusion, the phase-averaged concentration equation in a two-dimensional flow can be written

$$\frac{\partial \tilde{c}}{\partial t} + \frac{\partial \tilde{u}\tilde{c}}{\partial x} + \frac{\partial \tilde{w}\tilde{c}}{\partial z} = -\frac{\partial \widetilde{u'c'}}{\partial x} - \frac{\partial \widetilde{w'c'}}{\partial z} + w_f \frac{\partial \tilde{c}}{\partial z}. \tag{4}$$

In (4), the tilde is an operator to take a phase average; the instantaneous fluid particle velocities u and w and the sediment concentration c are separated into the sum of an organized and a turbulent contribution, i.e., $u = \tilde{u} + u'$, $w = \tilde{w} + w'$, $c = \tilde{c} + c'$. The mean flow is the organized wave-induced flow which includes both the undertow and the orbital wave motion, i.e., $\tilde{u} = \overline{u} + u_w$, $\tilde{w} = \overline{w} + w_w$ where the overbar is an operator to take a time average and the subscript w denotes the wave component. Equation (4) shows that the mass flux in the x direction is due to convection by mean flow, $\tilde{u}\tilde{c}$, and transport by turbulent velocity fluctuations, $\widetilde{u'c'}$, while the tendency of sediment to settle out is counteracted by the action of

turbulent fluctuations. Considering the common assumption of turbulent energy stirring up sediment and making it available for transport by the mean flow, the relationship between mean flow and turbulent kinetic energy is important. It would be interesting to investigate the relations between $\tilde{u}$ and k, where k is the turbulent kinetic energy, defined as

$$k = \frac{1}{2}(\widetilde{u'^2} + \widetilde{v'^2} + \widetilde{w'^2}). \tag{5}$$

The relative magnitude of $\widetilde{u'^2}$, $\widetilde{v'^2}$ and $\widetilde{w'^2}$ depends on the nature of the flow (Svendsen 1987). In breaker-generated turbulence, laboratory measurements have confirmed that the u' component has more energy than the other components. In this paper, we examine the correlation between $\tilde{u}$ and $(1/2)\widetilde{u'^2}$. We define a cross-correlation function, $R_{\tilde{u}k}$, as

$$R_{\tilde{u}k} = \frac{1}{2M}\sum_{i=1}^{M} \tilde{u}_i \widetilde{u_i'^2} \tag{6}$$

where $\tilde{u}_i$, $\widetilde{u_i'^2}$, $i = 1, \ldots, M$ are the M data values of $\tilde{u}$ and $\widetilde{u'^2}$ calculated using phase averaging. Considering the process of sediment entrainment by breaking waves we expect that $R_{\tilde{u}k}$ would be related to $\tilde{u}\tilde{c}$. Hence, the cross-correlation function between $\tilde{u}$ and $\frac{1}{2}\widetilde{u'^2}$ may be used as a measure of the cross-shore transport asymmetry where the signs of $R_{\tilde{u}k}$ indicate the predominant direction of transport. It is important to note that the cross-correlation function, $R_{\tilde{u}k}$, is related to the time-mean turbulent kinetic energy transport by the mean flow, $\overline{\tilde{u}k}$.

3. Experimental results

3.1. Spilling waves

A fundamental limitation of the LDA is that the sensor measures velocities at only one point in space. The complete velocity field is constructed by repeating

the same experiment many times and moving the probe to a succession of points across the flow field. In addition, turbulent velocity fluctuations are obtained by phase-averaging the velocity signal over many successive waves and then subtracting from the velocity signal the phase-averaged velocity. Therefore, highly reproducible waves are essential to ensure repeatability of test conditions and high quality of turbulent measurements. Fig. 3a shows the repeatability of the wave before the point of breaking. The phase average of water surface elevation taken from one hundred and two successive waves is compared to the first wave in the wave record. The traces are very near to being identical when inspected visually. Because wave breaking is a non-deterministic process the time history of water surface elevation in the surf zone will vary considerably from wave to wave; this is illustrated in Fig. 3b. Comparing Fig. 3b to Fig. 3a, the decay in wave height due to wave breaking is clearly apparent.

Fig. 4 shows the distributions of wave amplitudes and mean water level in the spilling breaker. The abscissa is the distance x measured positive shoreward from the toe of the slope. For the ordinate, the mean water level $\overline{\zeta}$ is measured from the undisturbed water surface, whereas the maximum and minimum water surface elevations $\zeta_{\max}$ and $\zeta_{\min}$ are measured from the mean water level. In Fig. 4, the value of wave height to mean water depth ratio is 0.82 at the breaking point ($x_b = 6.4\,\mathrm{m}$, $d_b = 19.6\,\mathrm{cm}$, $H_b = 16.25\,\mathrm{cm}$, $\overline{\zeta}_b = 0.29\,\mathrm{cm}$) and decreases with the decrease in water depth. The wave height remains an approximate fixed proportion of the mean water depth in the inner region of the surf zone where the height to depth ratio of the turbulent bore is about 0.5 ($x = 11.5\,\mathrm{m}$, $d = 4.93\,\mathrm{cm}$, $H = 3.38\,\mathrm{cm}$, $\overline{\zeta} = 1.87\,\mathrm{cm}$). As the wave propagates shoreward at locations past breaking, the decrease in momentum due to the wave decay is balanced by an increase in the mean water level. The slope of the mean water

level is seen to decrease in the inner region of the surf zone as found in previous studies (e.g. Stive and Wind, 1982).

Laboratory measurements of undertow have been conducted by Hansen and Svendsen (1984), Stive and Wind (1986), Nadaoka (1986) and Okayasu et al. (1988), amongst others. The driving mechanism for the undertow is the mismatch at each location in the vertical between the momentum flux gradient due to the breaking waves and the pressure gradient from the wave set-up, with the difference between these two forces being balanced by the turbulent shear stresses created by the undertow current. Fig. 5 shows the variations of time-mean horizontal velocity with depth at several locations in the wave tank. The position of each set of measurements is indicated by the normalized distance from the breaking point $(x - x_b)/h_b$ and the relative water depth h/h_b, where h is the local mean water depth, x_b and h_b are the x coordinate and the mean water depth at the breaking point, respectively. The undertow $\overline{u}$ is normalized by the wave celerity C, where $C = \sqrt{gh}$.

Outside the surf zone turbulence intensities are weak, Lagrangian mass transport is balanced by a return flow below trough level to maintain conservation of mass in the wave tank. The magnitude of this return flow decreases with distance from the surface and approaches zero near the bottom. Similarly, inside the surf zone the time-mean horizontal velocity is in the onshore direction near the surface and in the offshore direction below the trough level. However, the magnitude of return flow in the surf zone increases as z decreases with a very pronounced seaward current in the bottom region. The water carried landward by the breaking waves is returned below the trough level by the undertow. For example, at $(x - x_b)/h_b = 16.709$ $(h/h_b = 0.563)$, which is in the inner region of the surf zone, the time-mean horizontal velocity measured at $(z - \overline{\zeta})/h = -0.834$

is $-0.1C$. These results are consistent with previous studies.

Also plotted in Fig. 5 are the undertow measurements from Hansen and Svendsen (1984). They used a plane slope of 1 on 34.25. The water depth in front of the sloping beach was 36 cm, the wave period was 2.0 s, the wave height in the horizontal section of the wave flume was 12 cm, and the ratio H_0/L_0 was 0.192. Hence, the flow conditions in these two studies are almost identical. Indeed, we repeated their experiments first to verify our experimental methods. From Fig. 5 it is seen that the agreement with their results is very good. It is important to note that Hansen and Svendsen (1984) measured water particle velocities using a bi-directional micro-propeller current meter therefore turbulent velocities were not obtained. The results of this present study provide substantial details on surf zone turbulence that is not available in Hansen and Svendsen (1984).

Fig. 6 shows the variations of time-mean horizontal component of turbulent velocity with depth at several locations in the wave tank. Outside the surf zone the flow is predominantly laminar, and the turbulent velocity fluctuations are small compared to mean flow. In the region immediately after breaking, turbulence intensities throughout the water column increase steadily in the onshore direction. Visual observations reveal that the area of entrained air grows as aerated water spills down the front face of the wave. The vortices generated in the wave front are initially two-dimensional and in the spanwise direction (surface rollers). These large eddies break down through the formation of three-dimensional vortices extending obliquely downward, but turbulent flow is not established for a distance of several breaker depths. For example, at $(x - x_b)/h_b = 4.397$ $(h/h_b = 0.879)$ the bubble mass is growing rapidly behind the wave front but air bubbles are not seen below trough level, whereas

at $(x - x_b)/h_b = 7.462$ $(h/h_b = 0.809)$ entrained air bubbles transported by obliquely descending eddies are seen to reach the bottom. Fig. 6 shows that turbulent velocities in the surf zone decrease with distance from the surface. The experimental results are consistent with the common assumption that in the surf zone the primary turbulence mechanism is breaker-generated turbulence in the nearest proximity of the surface rollers, while turbulence generated by the organized wave-induced flow itself is weak and therefore turbulent energy below trough level is largely due to spreading of turbulence from the surface toward the bottom. It is noted that because fluid velocities are equal to zero when the probe is above the water surface, the time-mean turbulent velocity over one wave period actually decreases with distance above the trough level.

The time-mean turbulent kinetic energy in the surf zone is presented in Fig. 7a. Because the transverse velocity component is not measured, the turbulent kinetic energy is estimated as $k = (1.33/2)\left(\widetilde{u'^2} + \widetilde{w'^2}\right)$ after Stive and Wind (1982), and Svendsen (1987). The important thing to note is that the normalized turbulent energy $(\overline{k}/gh)^{\frac{1}{2}}$ varies only slowly with the water depth in the inner surf zone. This observation is consistent with measurements published by previous researchers. For example, the measurements by Stive (1980), and Stive and Wind (1982) are plotted in Fig. 7b. Their results were plotted in this type of graph by Svendsen (1987). The data shown is for a wave period of 1.79 s and a wave steepness H_0/L_0 of 0.032 (test 1). The beach slope was 1 on 40. Breaker type can be classified by the surf similarity parameter $\xi_0 = m/(H_0/L_0)^{\frac{1}{2}}$, where m is the beach slope. The value of ξ_0 for the spilling breaker in this present study is 0.20, while ξ_0 equals 0.14 in Stive (1980), and Stive and Wind (1982). From Figs. 7a and 7b it may be observed that the results are comparable for these similar wave conditions.

Phase averages of water surface elevation, horizontal velocity and turbulent velocity for a developed turbulent bore are shown in Figs. 8–10. The measurements were taken at $(x - x_b)/h_b = 16.709$ $(h/h_b = 0.563)$; the local wave height is 6.4 cm, the wave set-up is 1.34 cm, and the mean water depth is 11.2 cm. In Fig. 8, water surface elevation is measured relative to the mean water level. It is seen that phase averages of water surface elevation from different experiments are very near to being identical, which confirms both the repeatability of the experiments and the consistency of the capacitance wave gage measurements. The water surface elevation has the typical "saw-tooth" profile found in the inner region of the surf zone, in which the front face of the wave is much steeper than the back face.

The horizontal velocities are presented in Fig. 9. The trough level is located between $(z-\overline{\zeta})/h = -0.209$ and $(z-\overline{\zeta})/h = -0.298$. It is seen that the horizontal velocities are in phase with the surface elevation. The velocity measured at $(z - \overline{\zeta})/h = -0.209$ is zero during that part of the wave cycle when the probe is above the water surface. However, the "drop-out" is not abrupt because the water surface elevation varies considerably from wave to wave in the surf zone as shown in Fig. 3b.

Fig. 9 shows that the variation of horizontal velocity with distance from the surface is small under the wave trough. The maximum water particle speeds are attained under the wave trough and measure about $0.25C$, where C is the wave celerity based on the local mean water depth. During the forward wave velocities, the speeds are considerably lower; water particle speeds under the wave crest are about $0.2C$ at the trough level and decrease with distance from the surface. In addition, offshore motion is maintained for a longer period of time than onshore motion. This is due to the undertow current. From Fig. 5 it is seen that the

magnitude of the undertow increases from $0.017C$ at $(z-\overline{\zeta})/h = -0.298$ to $0.1C$ at $(z-\overline{\zeta})/h = -0.834$. Hence, we should expect that sediment suspended during wave breaking will be acted upon predominantly by an offshore water particle velocity field if it stays in the water column for a long time compared to the wave period. Above the trough level, fluid velocities under the wave crest increase in the direction of the free surface. However, if it is assumed that suspended sediment concentrations decrease with distance from the bottom then the effects of the surface roller on the rates and direction of sediment transport should be small. Thus, it is expected that the net movement of fine sediment would be seawards for this flow condition.

Fig. 10 shows that the temporal variation over a wave period of the turbulent velocity at a fixed point below trough level is small compared to the time-mean turbulent velocity. This is consistent with a turbulence decay time that is large compared to the wave period. The decay time of the large eddies should be proportional to the time scale of transfer of energy from large eddies to small eddies. Assuming large eddies lose a significant fraction of their kinetic energy within one "turnover time" (Tennekes and Lumley, 1972), the decay time of the large eddies should be proportional to ℓ/U, where ℓ and U represent the length and velocity scales of the large eddies. Taking $U \approx 0.05C$, $\ell \approx h$, the turbulence decay time is of order 2 s which is comparable to the wave period. Thus only a small portion of the energy generated in the spilling breaker is dissipated over one wave period. From Fig. 6 it is seen that the time-mean horizontal turbulent velocity decreases from $0.078C$ at $(z-\overline{\zeta})/h = -0.298$ to $0.052C$ at $(z-\overline{\zeta})/h = -0.834$. The turbulence intensities near the bottom are at their lowest at $t/T = 0$ (wave trough) and increase gradually as the wave crest passes. Turbulence intensities are at their highest shortly after $t/T = 0.5$ and decay

slowly over the backward stroke of the wave. Figs. 9 and 10 show that there is a phase difference between the phase-averaged horizontal velocity and the phase-averaged turbulent velocity, and this phase difference decreases upward. Near the water surface a high intensity turbulent core exists behind the breaking wave front, followed by progressively decreasing turbulent intensity regions towards the back face of the wave. The observed phase lags in the temporal variations of turbulent energy are consistent with the common assumption that turbulence is generated in the wave crest and spreads to the bottom by convection and/or turbulent diffusion.

The relations between mean flow and turbulence in the spilling breaker can be elucidated further based on the correlation between $\tilde{u}$ and $(1/2)\widetilde{u'^2}$. The variations of $R_{\tilde{u}k}/(gh)^{\frac{3}{2}}$ with depth at several locations in the inner region of the surf zone are shown in Fig. 11. The important thing to note is that the cross-correlation function is related to the time-mean turbulent kinetic energy transport by the organized wave-induced flow $\overline{\tilde{u}k}$. To a first order approximation, it is expected that suspended sediment concentration is proportional to turbulence intensity in the surf zone. Hence, suspended sediment transport $\tilde{u}\tilde{c}$ superficially resembles turbulence transport $\tilde{u}k$ and the signs of the cross-correlation function may be used to predict the predominant directions of sediment transport. It is seen that the correlations between mean flow and turbulence indicate a generally seaward correlation below the trough level (i.e. $R_{\tilde{u}k} < 0$). Also shown in Fig. 11 are the correlations between $\overline{u}$ and $(1/2)\widetilde{u'^2}$. The mean flow is the organized wave-induced flow which includes both the undertow and the orbital wave motion, i.e, $\tilde{u} = \overline{u} + u_w$. It is seen that the two results are very close below trough level, which means that the correlations there are mainly due to the undertow. The results in Fig. 11 indicate that in the spilling breaker the

undertow is more important in transporting sediment, and the net transport is offshore.

3.2. Plunging waves

To investigate the effects of breaker type on the flow in the surf zone the wave height in the constant-depth region of the wave tank was kept the same, i.e., about 13 cm, while the wave period was increased from 2.0 s to 5.0 s. The value of wave height to wavelength ratio in deep water, H_0/L_0, is thus decreased from 0.020 to 0.0023, and the breaking behaviour changes from spilling breaking to plunging breaking. It is noted that all the detailed velocity measurements in breaking waves published to date have been conducted with much larger values of H_0/L_0. Because of this, the differences observed between spilling and plunging breakers are not distinct. In this study, striking differences are found in the details of the flow in the bore region, which can be related to the processes of wave breaking in the spilling and plunging waves.

Fig. 12 shows the distribution of wave amplitudes and mean water level in the plunging breaker. At the breaking point ($x = 7.795$ m), the wave height is 19.0 cm, the still water depth is 15.6 cm and the wave set-up is -0.25 cm. In the bore region ($x = 12.0$ m), the wave height is 4.35 cm, the still water depth is 3.77 cm and the wave set-up is 1.69 cm. Comparing Fig. 12 to Fig. 4, the value of wave height to water depth ratio has increased from 0.82 to 1.20 at the breaking point and from 0.5 to 0.8 in the inner region of the surf zone. The slope of the wave set-up is also larger in the plunging breaker than in the spilling breaker.

The large difference in wave height to water depth ratio observed between the spilling and plunging breakers should not be passed over lightly. The ratio H/h is a measurable quantity which can be used to distinguish the types of

breaker. This parameter may also be related to the production and spreading of turbulent kinetic energy. Surf zone turbulence originates from instabilities of the surface waves. The large-scale turbulence is created by wave breaking and the large-scale motions contribute most to the turbulent transport of energy and momentum. Hence, the dynamics of turbulence in the surf zone should have certain unique characteristics that are associated with a particular wave condition. Indeed, significant differences are found between the characteristics of mean flow and turbulence in the spilling and plunging breakers; this will be discussed more fully later.

Variations of time-mean horizontal velocity with depth are shown in Fig. 13. Comparing Fig. 13 to Fig. 5, it is seen that in the surf zone the magnitude of undertow in the bottom region in the plunging breaker is generally less than that in the spilling breaker, though the wave height to water depth ratios are larger. For example, at $(x - x_b)/h_b = 16.883$ $(h/h_b = 0.584)$, the time-mean horizontal velocity at $(z - \overline{\zeta})/h = -0.789$ is $-0.089C$, while it was about $-0.1C$ for the spilling breaker. It is seen that the magnitude of undertow current is virtually constant over the depth between the trough level and the bottom boundary layer. This is different from the spilling breaker where the undertow current increases with distance from the surface until the boundary layer. It is conjectured that the mixing of momentum causes the undertow under the plunging breaker to be much more uniform. This effect is also observed in the experiments of Okayasu et al. (1988). The results of their case 2 is plotted in Fig. 14. In their experiment, the wave period was 2.0 s, the incident wave height was 5.63 cm at 40 cm depth, and the bed slope was 1 on 20. The ratio H_0/L_0 was 0.0092 thus the surf similarity parameter ξ_0 was 0.52, while the value of ξ_0 in this present study is 0.6. Comparing Fig. 13 to Fig. 14 it may be observed

that the time-mean horizontial velocities are not the same but are of the same order of magnitude, and the variations over depth of the undertow current are small in both studies.

Fig. 15 shows the variations of time-mean horizontal component of turbulent velocity with depth at several locations on the slope. At $h/h_b = 1.078$, the shoaling wave is approaching breaking but instability has not yet developed in the wave crest. The turbulent velocity fluctuations are small compared to the mean flow. At $h/h_b = 1.0$ the front face of the wave has become vertical and the wave front begins to curl forward; the fluid motion under the wave is not turbulent. At $h/h_b = 0.929$, the jet from the overturning wave front plunges into the oncoming trough and the violent transition to rotational flow begins. The bubble mass is still quite small and there are some fluctuations in the position of jet impact. As the air entrapped by the impinging jet mixes with the water, a region of high vorticity (plunger vortex) and concentration of air bubbles develops. The bubble mass in the plunger vortex rises gradually and propagates along with the wave past the probe at $h/h_b = 0.857$. Turbulence intensities over the entire water column increase rapidly with wave propagation distance as the ordered vortex motions degenerate into small-scale motion with increasing disorder. At the same time, the impact of the jet causes water to splash up and forms another jet which strikes the water ahead of the probe at $h/h_b = 0.857$. The air entrapped by the second jet impact fills the entire water column with air bubbles which then travel forward with the propagating wave. At $h/h_b = 0.773$ the broken wave resembles a turbulent bore, but small splashes and plunger vortices can still be seen. The horizontal distance between this location and that of the initial jet impact is approximately six times the undisturbed water depth at the breaking point. In comparing the bubble mass

area in the inner surf zone in the plunging breaker to that observed in the spilling breaker, air bubbles fill the entire water column in the plunging breaker whereas air bubbles are sporadic in the bottom region in the spilling breaker. This means that vertical mixing is much stronger in the plunging breaker than in the spilling breaker. Comparing Fig. 15 to Fig. 6, it is seen that there is virtually no vertical variation in turbulence intensities below trough level in the plunging breaker, whereas turbulent velocity decreases from the trough level to the bottom in the spilling breaker.

The plunging breaker in this present study differs from those of previous studies (e.g. Stive 1980, Stive and Wind 1982, Okayasu et al. 1986) in the wave breaking condition. In the afore-mentioned studies plunging breakers have been used and turbulence intensities have been measured at various locations in the surf zone. Stive (1980), and Stive and Wind (1982) used a plane beach of slope 1 on 40, and the value of H_0/L_0 in their test 2 was 0.01. This yields a surf similarity parameter ξ_0 of 0.25. The measurements of Okayasu et al. (1986) were made on a plane beach of slope 1 on 20 and the value of H_0/L_0 in their case 2 was 0.0226 thus the value of ξ_0 was 0.33. The value of ξ_0 in our plunging breaker is 0.60 which is much larger than those used in previous studies. Because of this, the value of H/h in the inner surf zone is also larger, e.g., 0.8 in this present study compared to 0.54 in Stive 1980. A comparison with the data from Stive (1980) and Stive and Wind (1982) is made in Fig. 16. It is seen that at large value of ξ_0 wave breaking is so intense that the turbulence intensities are much higher.

Phase averages of water surface elevation, horizontal velocity and turbulent velocity in the bore region are shown in Figs. 17–19. The measurements were taken at $(x - x_b)/h_b = 16.883$ $(h/h_b = 0.584)$. The local wave height is 7.21 cm,

the wave set-up is 1.1 cm, and the mean water depth is 9.0 cm. The "saw-tooth" profile of the water surface elevation has a secondary crest behind the wave front which is not found in the spilling breaker. This is not apparent outside the surf zone and is seen to originate from the impact of the overturning wave front at breaking. Visual observations show that bubble mass in the plunging breaker occupies the full depth. The strong mixing of momentum and the smaller water depth to wavelength ratio cause the velocity field to be much more uniform; variations of horizontal velocities and turbulent velocities with water depth are significant only in the front roller. Water particle velocities under the trough are approximately $-0.4C$, whereas under the crest they vary from $0.2C$ near the bottom to $0.4C$ at the trough level; the trough level is located at about $(z - \overline{\zeta})/h = -0.4$. This is different from the spilling breaker in which water particle speeds during the crest portion of the wave are considerably lower than water particle speeds during the trough portion. It is also seen that turbulent velocities in the plunging breaker vary greatly over a wave period. Turbulent energy is highest under the wave front and decays rapidly after the crest passes. This is consistent with a turbulence decay time that is small compared to the wave period. The decay time of large-scale vortices is proportional to ℓ/U. Taking $U \approx 0.2C$, $\ell \approx h$, the turbulence decay time is of order 0.5 s which is indeed much shorter than the wave period of 5.0 s. The short decay time is due to large eddies which have large velocity scales. It is noted that the phase lead of the maximum phase-averaged velocity over the maximum phase-averaged turbulent velocity seen in the spilling breaker does not occur in the plunging breaker. This indicates that vertical mixing is very rapid in the wave with the larger H/h. Because phase-averaged velocities and turbulent velocities are in phase and turbulence intensities are highest under the wave crest, there

would be an enhanced sediment transport during the forward stroke of the wave. Thus, it is expected that the net movement of sediment could be shorewards for this flow condition.

The variations of mean flow/turbulent energy correlation with depth at several locations in the inner region of the surf zone are shown in Fig. 20. It is seen that the correlations between mean flow and turbulence below the trough level are positive, while the correlations between the undertow and the turbulence are negative. However, the contributions of orbital wave motion dominate due to high turbulence intensities and onshore velocities under the wave crest. Therefore, the net transport of turbulent kinetic energy is onshore under the plunging breaker.

This study shows that turbulence transport by mean flow is different in spilling and plunging breakers. The observed results cannot be explained simply from the difference in wave period since turbulence plays a major role in this process. The turbulence time scale is associated with the large eddies created by wave breaking. The turbulence characteristics of spilling and plunging breakers are different because the ratios of turbulence time scale and wave period are different in these waves. This ratio affects how turbulent energy is transported by mean flow and turbulence thus changing the turbulence dynamics considerably. We expect that Froude scaling will apply for the large eddies as well as the organized wave-induced flow since the large-scale motions are created by instabilities of surface wave under the influence of gravity. Hence, the ratio of turbulence time scale and wave period should be independent of model scale so that the basic results hold in both small-scale and large-scale experiments. Indeed, Stive (1985) has shown that scale effects are not apparent in a laboratory surf zone.

4. Relationship with storm/normal beach profiles

This study has focused on surf zone dynamics in the inner and outer surf zone. Around the waterline swash zone dynamics and sheet flow transport are important and they are not addressed with these experiments. However, numerous laboratory and field studies have shown that Dean's heuristic model indeed distinguishes storm and normal profiles reasonably well. It was found that storm waves carry sand offshore to form offshore bars, while swell waves following a storm would transport sand from the offshore bars to be re-deposited on the forshore. The question is what physical mechanisms would produce this onshore/offshore transport of sediment across the surf zone. In this paper it is shown that the characteristics of turbulent flow are significantly different in spilling and plunging breakers. The correlations between mean flow and turbulence show that turbulent kinetic energy is transported seaward under a spilling breaker and landward under a plunging breaker. Much work remains to be done to understand the correspondence between sediment transport processes and dynamics of turbulent flow in controlled experiments over sand beaches. However, to a first approximation it may be expected that suspended sediment concentration in the surf zone is proportional to turbulence intensity. Hence, sediment transport superficially resembles turbulence transport. The findings of this study suggest that sediment transport and beach transformation may be tied in a direct way to the unique characterisitics of turbulent flow in different types of breaker. This would have a direct impact on the development of coastal models for predicting shoreline change.

It can be demonstrated that the spilling and plunging breakers studied here are related to storm (erosional) and normal (accretionary) beach profiles, respec-

tively. Assuming a median sand grain diameter of 0.3 mm, and a corresponding fall velocity w_f of 4 cm/s, we compute the value of H_0/L_0 that would separate the wave conditions into erosional and accretional regimes as given by Eq. (1). For the spilling breaker, the wave period T is 2.0 s, the deep-water wave steepness H_0/L_0 is 0.02. From Eq. (1), the value of H_0/L_0 is 0.011. Hence the wave condition is erosional for the spilling breaker, as suggested above by the examination of $R_{\tilde{u}k}$ shown in Fig. 11. For the plunging breaker, the wave period is 5.0 s, and the deep-water wave steepness is 0.0023. From Eq. (1), the value of H_0/L_0 is 0.0044. Thus the wave condition is accretional for the plunging breaker. These conclusions will hold provided that the value of w_f is in the range between 2 cm/s and 8 cm/s, or equivalently, the value of sand grain diameter is in the range between 0.2 mm and 0.5 mm.

The results are not conclusive if the profile parameter P, which is based on large-scale wave tank data, is used to analyze the waves studied here. Again we take a fall velocity of 4 cm/s. For the spilling breaker, we estimate a deep-water wave height $H_0 = 0.127$ m based on linear shoaling, giving $P = 1,236$. Thus the wave condition is accretional. However, the value of P is very sensitive to the value of w_f, since $P \propto w_f^{-3}$. For example, if we take a fall velocity of 2 cm/s, we get $P = 9,889$. This value puts the spilling breaker right on the dividing line between erosional and accretional wave conditions. For the plunging breaker, we estimate a deep-water wave height $H_0 = 0.089$ m, giving $P = 242$. This wave thus falls strongly in the accretional regime.

5. Conclusions

To examine the effects of breaker type on cross-shore transport laboratory experiments were carried out in which measurements of fluid velocities and sur-

face elevation were made on a uniformly sloping beach. Velocity measurements were made mainly below trough level and above bottom boundary layer. Experiments were conducted for a spilling breaker and a plunging breaker, which are representative of storm and swell waves, respectively. In the simplest situation, swell waves move sand onshore and produce an accretionary beach profile, whereas steep winter storm waves cut into the beach face and carry sand offshore to form offshore bars. The velocity field in each type of wave environment was studied with attention directed toward understanding the relationship between mean flow and turbulence in these waves. The following main conclusions can be drawn from this investigation:

1. Experimental measurements in the bore region of the spilling breaker show that the temporal variation of turbulent velocity is small. Below the trough level, the maximum water particle speeds are attained in the trough portion of the wave, whereas the water particle speeds during the crest portion of the wave cycle are considerably lower. In addition, offshore motion is maintained for a longer period of time than onshore motion. The correlations between mean flow and turbulence are seawards and dominated by the undertow current. The above results indicate a generally seaward directed suspended sediment transport under the spilling breaker for fine sediments.

2. Turbulent velocity measurements in the bore region of the plunging breaker show a peak under the wave crest followed by a rapid decline under the back face of the wave. Turbulent velocity under the wave crest is three to four times the turbulent velocity under the trough, whereas water particle speeds under the crest are only slightly smaller than those under the trough. The correlations between mean flow and turbulence are landwards and dominated by the orbital wave motion. The concurrence of high turbulence intensity

with high onshore water particle speed means that suspended sediment could be moved landward under the plunging breaker.

3. Mean flow velocity and turbulent intensity vary with distance from the surface in the spilling breaker. Vertical variations are not evident in the plunging breaker. Visual observations of bubble mass show that large-scale vortices create a strong vertical mixing of mass and momentum in the plunging breaker, whereas in the spilling breaker turbulence is spread gradually downward by moderate-scale eddies originating from the surface roller.

4. The present study shows that in spite of the similarities in wave profiles in the bore region the characteristics of turbulence structure and undertow are different in spilling and plunging breakers. Turbulent kinetic energy is transported seaward by mean flow under the spilling breaker and the dissipation rate is slow. This is different from the plunging breaker where turbulent kinetic energy is transported landward and dissipated within one wave cycle. The resemblence of turbulent bores from a plunging breaker to those originating from a spilling breaker may be understood as a depth-limited condition in which the height of the broken waves remains an approximate fixed proportion of the mean water depth. However, the value of H/h is much larger in the plunging breaker than in the spilling breaker. This ratio is a measurable quantity which may be related to the production and spreading of turbulence in breaking waves. Flow visualization indicates that the processes of transformation from organized wave motion into turbulent motion are fundamentally different in spilling and plunging breakers. Under the plunging breaker the turbulence generated seaward is transported landward by convection so that the turbulent flow pattern moving downstream is strongly dependent on its history. The resulting differences in the

relationship between mean flow and turbulence in these waves should become increasingly evident as the type of wave breaking goes from spilling to plunging to collapsing.

5. The initial comparison here of the correlation function $R_{\tilde{u}k}$ and the separation of erosional and accretional wave conditions based on Dean's heuristic model suggests that sediment transport and beach transformation may be tied in a direct way to the turbulence dynamics of the breaking wave, particularly to the relationship between ensemble-averaged horizontal velocity and turbulent kinetic energy. It is natural to expect this, if it is assumed that turbulence in the fluid column is effective in keeping sand in suspension after passage of a bore front. Much work remains to be done to demonstrate this correspondence in controlled experiments over a sand bed. At present, a somewhat simpler set of experiments are being conducted to further evaluate the correspondence between $R_{\tilde{u}k}$ and the separation of storm/normal wave conditions for a wider range of wave conditions, but with less detail in the vertical profile structure.

6. This study suggests that cross-shore sediment transport could be influenced greatly by the correlation between organized wave-induced flow and turbulence intensity. Therefore, predictive models of coastal processes must correctly model the spatial and temporal variations of turbulence and their relations to the mean flow to appropriately predict rates and direction of sediment transport. A comparison of mean and turbulent flow characteristics between spilling and plunging breakers indicates that the dynamics of surf-zone turbulence depends on a particular wave condition and it is not similar for different deep-water wave conditions. A detailed analysis of the dynamics of turbulence in spilling and plunging breakers is currently

underway and will be reported in the near future.

Acknowledgements

This study was funded by the Office of Naval Research under contract N-00014-90-J1678. F.C.K.T. also acknowledges the support of the Texas Higher Education Coordinating Board through Grant 999903-261. Dr. Robert A. Dalrymple is acknowledged for several helpful suggestions.

References

Barkaszi, S. F., Jr. and Dally, W. R., 1993. Fine-scale measurements of sediment suspension by breaking waves at Supertank. In: Proc. 23rd Intl. Coastal Eng. Conf., Venice, 1992. ASCE, New York, pp. 1910–1923.

Beach, R. A. and Sternberg, R. W., 1988. The influence of infragravity energy on suspended sediment transport in the inner surf zone. Mar. Geol., 80: 61–79.

Dalrymple, R. A., 1992. Prediction of storm/normal beach profiles. J. Waterw. Port Coastal Ocean Eng., ASCE, 118: 193–200.

Dean, R. G., 1973. Heuristic models of sand transport in the surf zone. In: Proc. Conf. on Eng. Dynamics in the Surf Zone, Institute of Engineers, pp. 208–214.

Downing, J. P., 1983. Field studies of suspended sand transport, Twin Harbors Beach, Washington. Ph.D. thesis, 121 pp.

Goring, D. G., 1978. Tsunamis: The propagation of long waves onto a shelf.

Report No. KH-R-38 W. M. Keck Laboratory of Hydraulics and Water Resources, California Institute of Technology, Pasadena, CA, 337 pp.

Hansen, J. B. and Svendsen, I. A., 1984. A theoretical and experimental study of undertow. In: Proc. 19th Intl. Coastal Eng. Conf., Houston, TX. ASCE, New York, pp. 2246–2262.

Jaffe, B. E., 1993. The contribution of suspension events to sediment transport in the surf zone. In: Proc. 23rd Intl. Coastal Eng. Conf., Venice, 1992. ASCE, New York, pp. 2680–2693.

Jaffe, B. E., Sternberg, R. W. and Sallenger, A. H., 1985. The role of suspended sediment in shore-normal beach profile changes. In: Proc. 19th Intl. Coastal Eng. Conf., Houston, TX. ASCE, New York, pp. 1983–1996.

Kraus, N. C. and Larson, M., 1988. Beach profile change measured in the tank for large waves, 1956–1957 and 1962. Tech. Report CERC-88-6, U.S. Army Corps. of Engrs. Coastal Engrg. Res. Ctr., Vicksburg, MS, 39 pp.

Kriebel, D. L., Dally, W. R. and Dean, R. G., 1986. Undistorted Froude scale model for surf zone sediment transport. In: Proc. 20th Intl. Coastal Eng. Conf., Taipei. ASCE, New York, pp. 1296–1310.

Larson, M. and Kraus, N. C., 1989. SBEACH: Numerical model for simulating storm-induced beach change. Tech. Report CERC-89-9 U.S. Army Corps of Engrs. Coastal Engrg. Res. Ctr., Vicksburg, MS, 256 pp.

Nadaoka, K., 1986. A fundamental study on shoaling and velocity field structure of water waves in the nearshore zone. Tech. Report. No. 36 Dept.

Civ. Engrg., Tokyo Inst. Tech., 125 pp.

Okayasu, A., Shibayama, T. and Nimura, N., 1986. Velocity field under plunging waves. In: Proc. 20th Intl. Coastal Eng. Conf., Taipei. ASCE, New York, pp. 660–674.

Okayasu, A., Shibayama, T. and Horikawa, K., 1988. Vertical variation of undertow in the surf zone. In: Proc. 21st Intl. Coastal Eng. Conf., Malaga. ASCE, New York, pp. 478–491.

Stive, M. J. F., 1980. Velocity and pressure field of spilling breakers. In: Proc. 17th Intl. Coastal Eng. Conf., Sydney. ASCE, New York, pp. 547–566.

Stive, M. J. F., 1985. A scale comparison of wave breaking on a beach. Coastal Eng., 9: 151–158.

Stive, M. J. F. and Wind, H. G., 1982. A study of radiation stress and set-up in the nearshore region. Coastal Eng., 6: 1–25.

Stive, M. J. F. and Wind, H. G., 1986. Cross-shore mean flow in the surf zone. Coastal Eng., 10: 325–340.

Svendsen, I. A., 1987. Analysis of surf zone turbulence. J. Geophys. Res., 92(C5): 5115–5124.

Svendsen, I. A., Madsen, P. A. and Buhr Hansen, J., 1978. Wave characteristics in the surf zone. In: Proc. 16th Intl. Coastal Eng. Conf., Hamburg. ASCE, New York, pp. 520–539.

Tennekes, H. and Lumley, J. L., 1972. A first course in turbulence. MIT Press, Cambridge, MA, 300 pp.

LIST OF TABLES

LIST OF FIGURES

Fig. 12. Distribution of wave amplitudes and mean water level in plunging breaker.

Fig. 13. Variation of time-mean horizontal velocity with depth in plunging breaker. (a) $(x-x_b)/h_b = -3.247$, $h/h_b = 1.078$. (b) $(x-x_b)/h_b = 0.0$, $h/h_b = 1.0$. (c) $(x-x_b)/h_b = 3.571$, $h/h_b = 0.929$. (d) $(x-x_b)/h_b = 6.494$, $h/h_b = 0.857$. (e) $(x-x_b)/h_b = 9.740$, $h/h_b = 0.773$. (f) $(x-x_b)/h_b = 12.987$, $h/h_b = 0.675$. (g) $(x-x_b)/h_b = 16.883$, $h/h_b = 0.584$.

Fig. 14. Time-mean horizontal velocity from case 2 of Okayasu et al. (1988); $h/h_b = 0.71$ ($\circ$), $h/h_b = 0.4$ ($\times$).

Fig. 15. Variation of time-mean horizontal turbulent velocity with depth in plunging breaker. (a) $(x-x_b)/h_b = -3.247$, $h/h_b = 1.078$. (b) $(x-x_b)/h_b = 0.0$, $h/h_b = 1.0$. (c) $(x-x_b)/h_b = 3.571$, $h/h_b = 0.929$. (d) $(x-x_b)/h_b = 6.494$, $h/h_b = 0.857$. (e) $(x-x_b)/h_b = 9.740$, $h/h_b = 0.773$. (f) $(x-x_b)/h_b = 12.987$, $h/h_b = 0.675$. (g) $(x-x_b)/h_b = 16.883$, $h/h_b = 0.584$.

Fig. 16. Variation of turbulent kinetic energy with depth in plunging breaker. (a) present experiment; $h/h_b = 0.929$ (+), 0.857 ($*$), 0.773 ($\circ$), 0.675 ($\times$), 0.584 ($\bullet$). (b) test 2 of Stive and Wind (1982); 0.905 (+), 0.709 ($*$), 0.544 ($\circ$), 0.381 ($\times$), 0.143 ($\bullet$).

Fig. 17. Phase-averaged surface elevations for plunging breaker at $(x-x_b)/h_b = 16.883$ and $h/h_b = 0.584$. The curves are from different experiments with identical test conditions.

Fig. 18. Phase-averaged horizontal velocities for plunging breaker at $(x-x_b)/h_b = 16.883$ and $h/h_b = 0.584$; $(z-\overline{\zeta})/h = -0.456$ (—), -0.567 ($--$), -0.678 ($-.$), -0.789 ($\cdots$).

Fig. 19. Phase-averaged horizontal turbulent velocities for plunging breaker at $(x-x_b)/h_b = 16.883$ and $h/h_b = 0.584$; $(z-\overline{\zeta})/h = -0.456$ (—), -0.567 ($--$), -0.678 ($-.$), -0.789 ($\cdots$).

Fig. 20. Variation of cross correlation function with depth for plunging breaker; correlation between mean flow and turbulence ($\circ$), correlation between undertow and turbulence ($\times$). (a) $h/h_b = 0.857$. (b) $h/h_b = 0.773$. (c) $h/h_b = 0.675$. (d) $h/h_b = 0.584$.

Table 1
Wave conditons (the subscripts 0, h and b denote deep water, horizontal region and breaking point)

Breaker type	H_0 (m)	H_h (m)	T (s)	H_0/L_0	x_b (m)	d_b (m)		
Spilling	0.127	0.125	2.0	0.020	6.400	0.196		
Plunging	0.089	0.128	5.0	0.0023	7.795	0.156		
Locations of measurements and water depths								
Spilling breaker								
x (m)	−1.265	5.945	6.665	7.275	7.885	8.495	9.110	9.725
d (m)	0.400	0.208	0.185	0.169	0.152	0.137	0.119	0.097
h (m)	0.400	0.212	0.192	0.175	0.161	0.148	0.133	0.112
Plunging breaker								
x (m)	7.295	7.795	8.345	8.795	9.295	9.795	10.395	
d (m)	0.169	0.156	0.142	0.128	0.113	0.096	0.079	
h (m)	0.166	0.154	0.143	0.132	0.119	0.104	0.090	

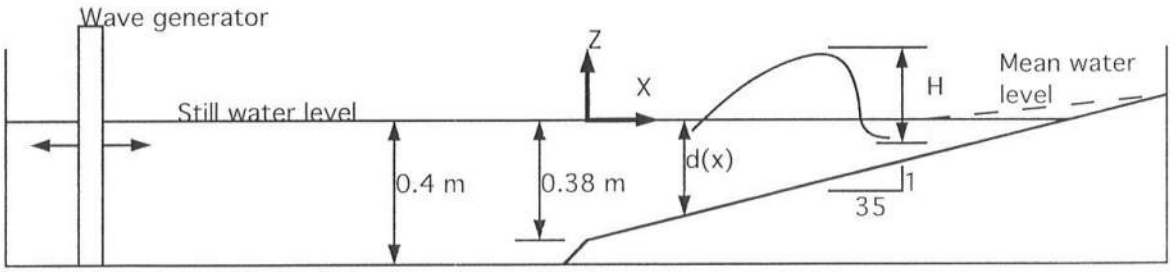
Wave generator
Z
X
H
Mean water level
Still water level
0.4 m
0.38 m
d(x)
1
35

FIGURE 1

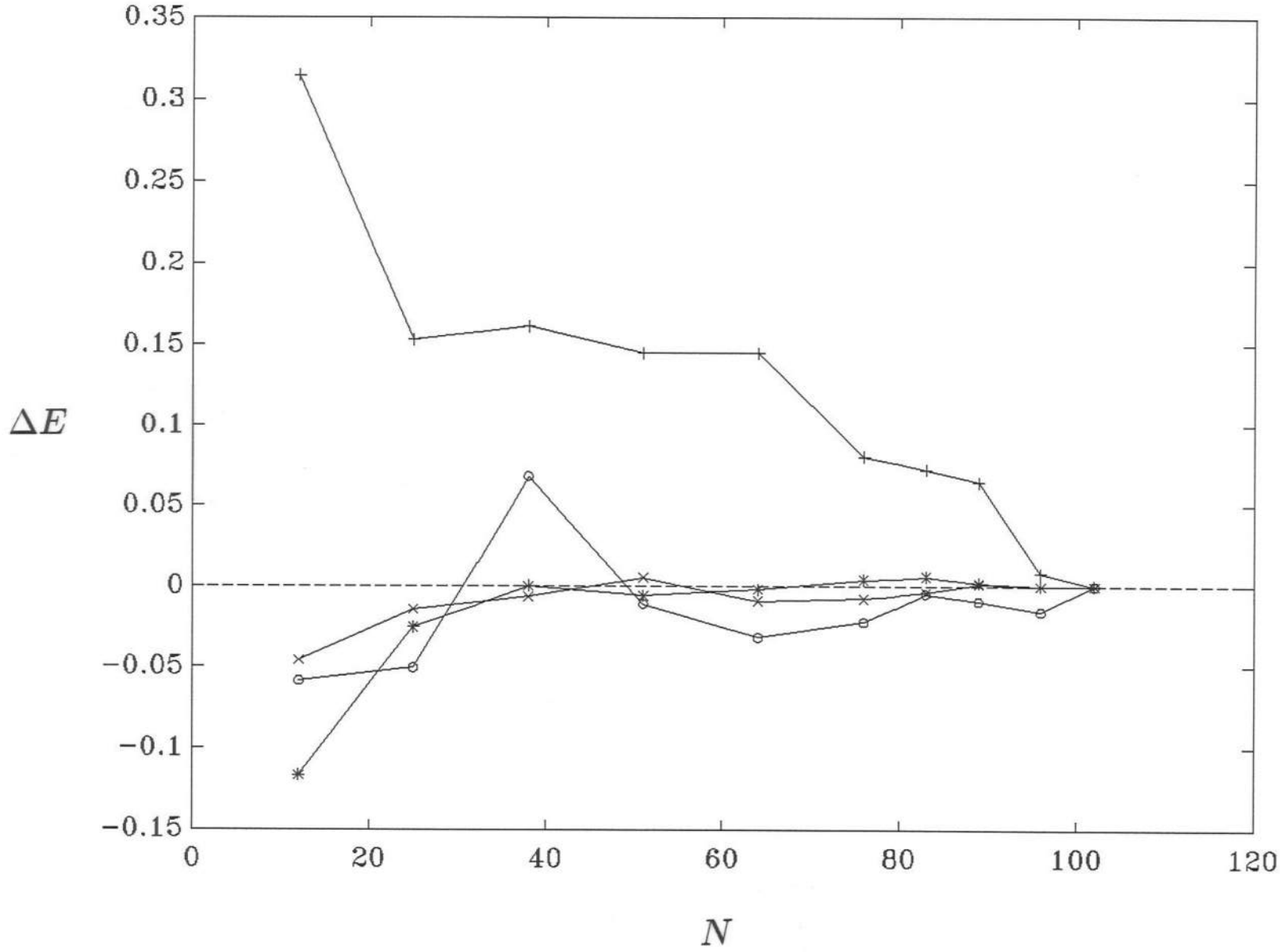

FIGURE 2

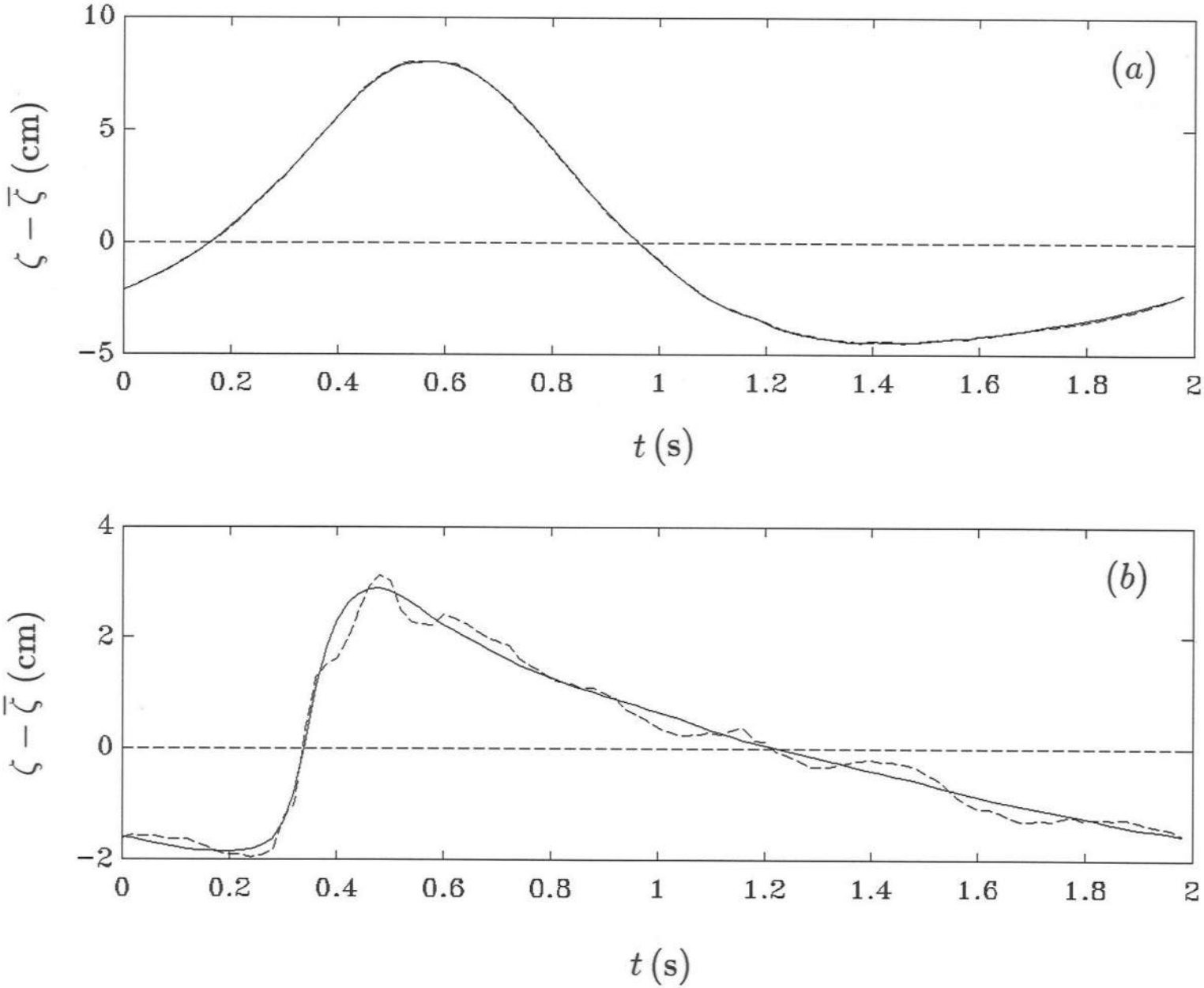
(a)
10
5
0
−5
0
0.2
0.4
0.6
0.8
1
1.2
1.4
1.6
1.8
2
$\zeta - \overline{\zeta}$ (cm)
t (s)
(b)
4
2
0
−2
0
0.2
0.4
0.6
0.8
1
1.2
1.4
1.6
1.8
2
$\zeta - \overline{\zeta}$ (cm)
t (s)

FIGURE 3

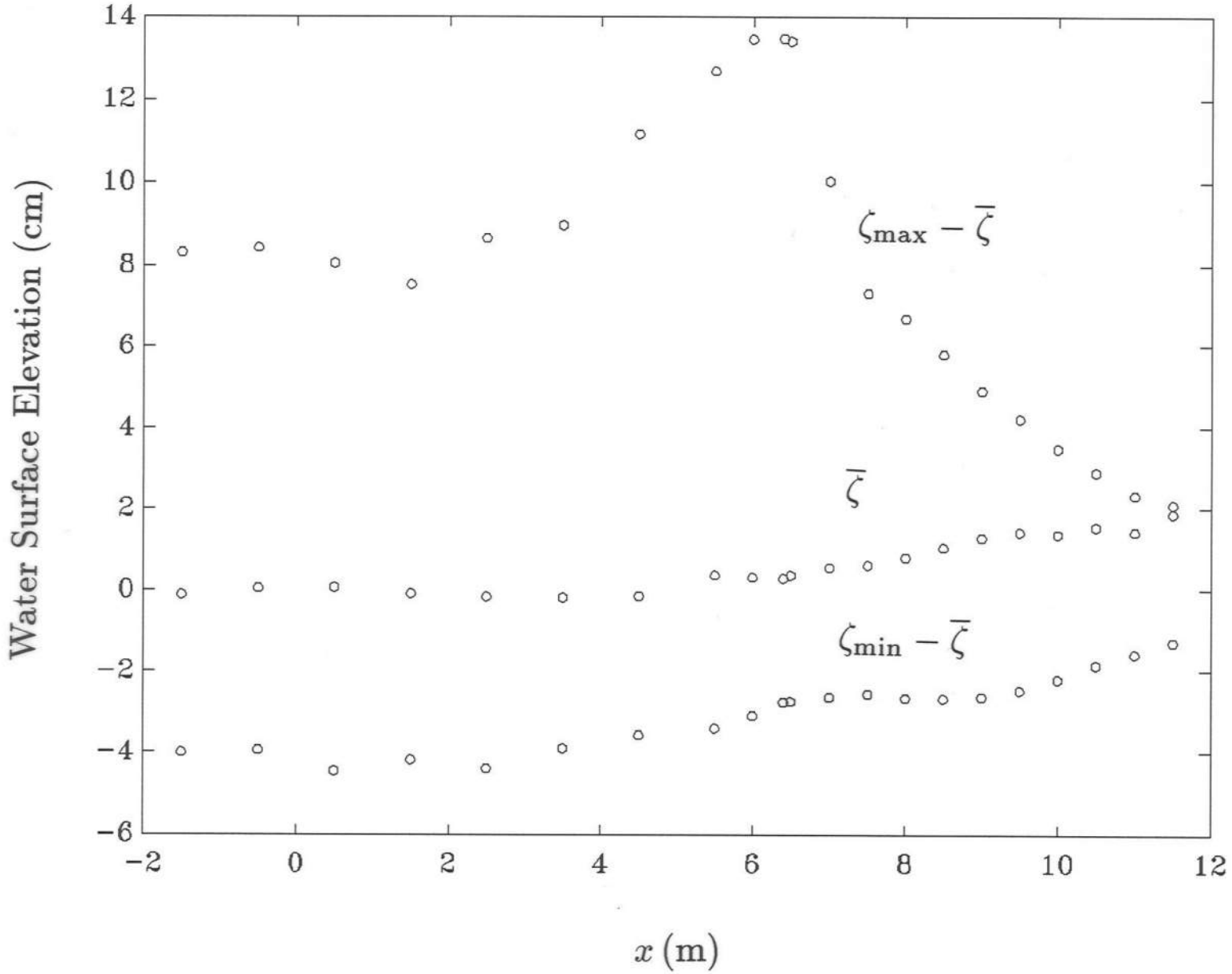
Water Surface Elevation (cm)
14
12
10
8
6
4
2
0
−2
−4
−6
−2
0
2
4
6
8
10
12
x (m)
$\zeta_{max} - \overline{\zeta}$
$\overline{\zeta}$
$\zeta_{min} - \overline{\zeta}$

FIGURE 4

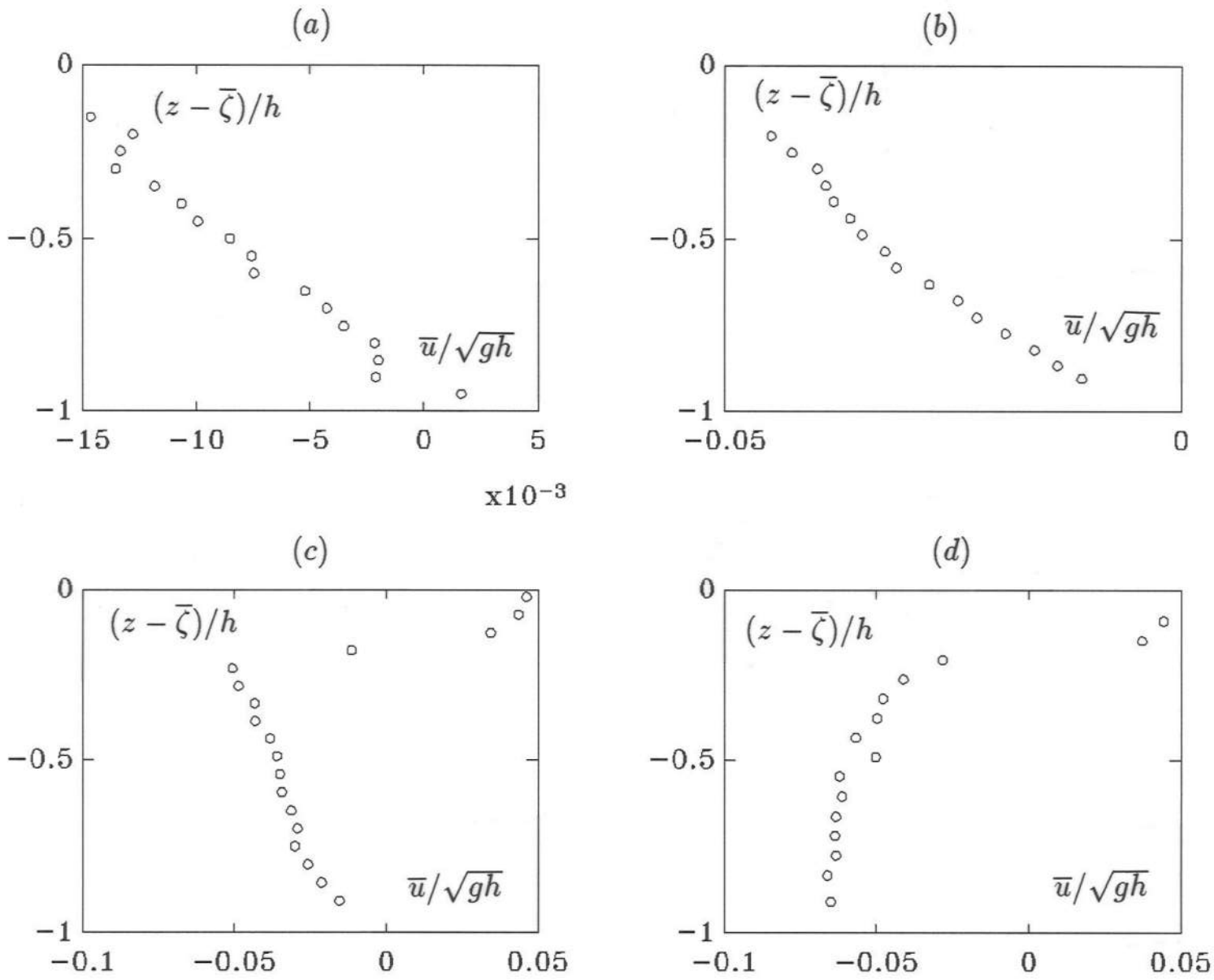
(a)
(b)
(c)
(d)
$(z-\overline{\zeta})/h$
$\overline{u}/\sqrt{gh}$
0
−0.5
−1
−15
−10
−5
0
5
x10^{-3}
−0.05
−0.1
0.05

FIGURE 5

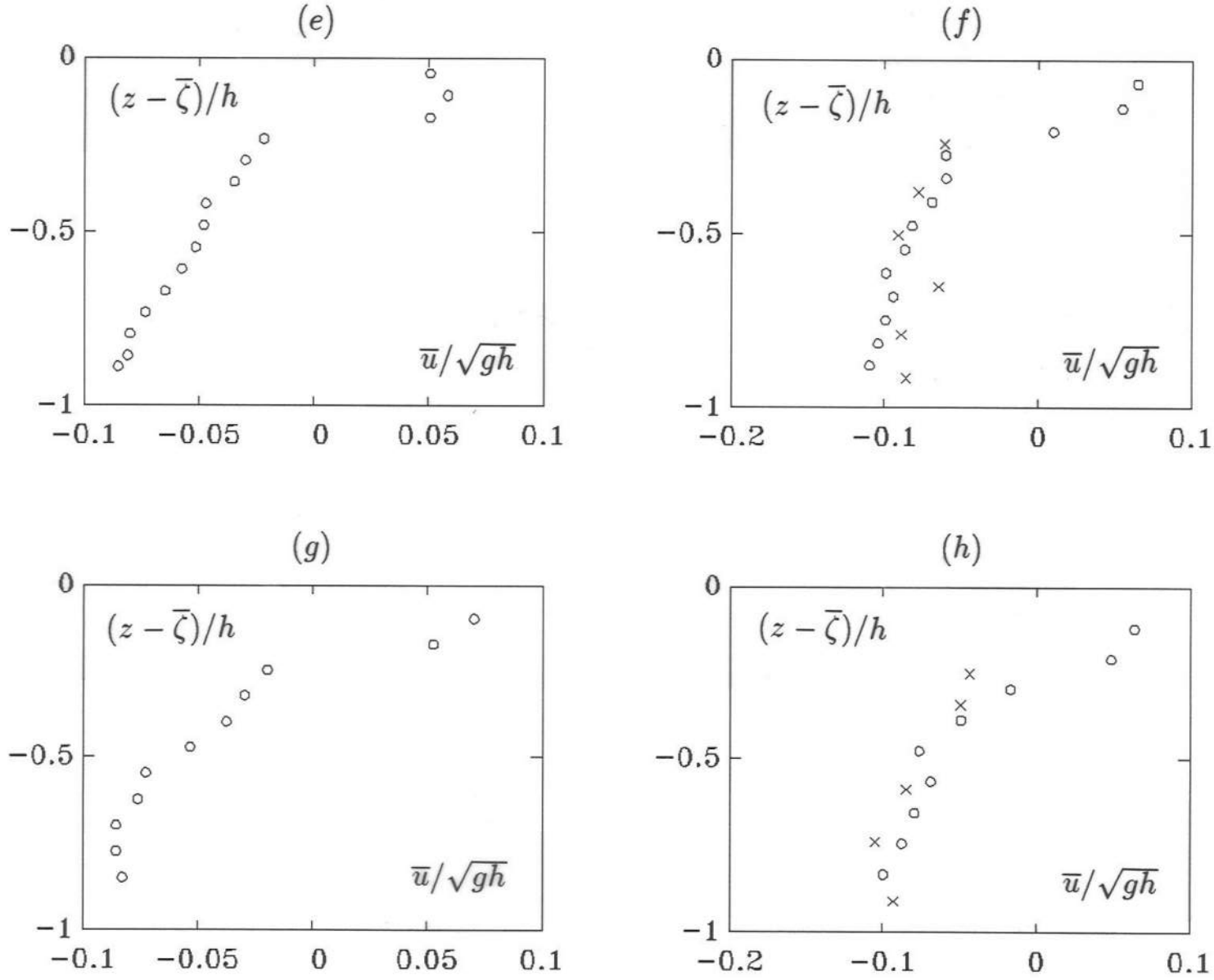

FIGURE 5 (Continued)

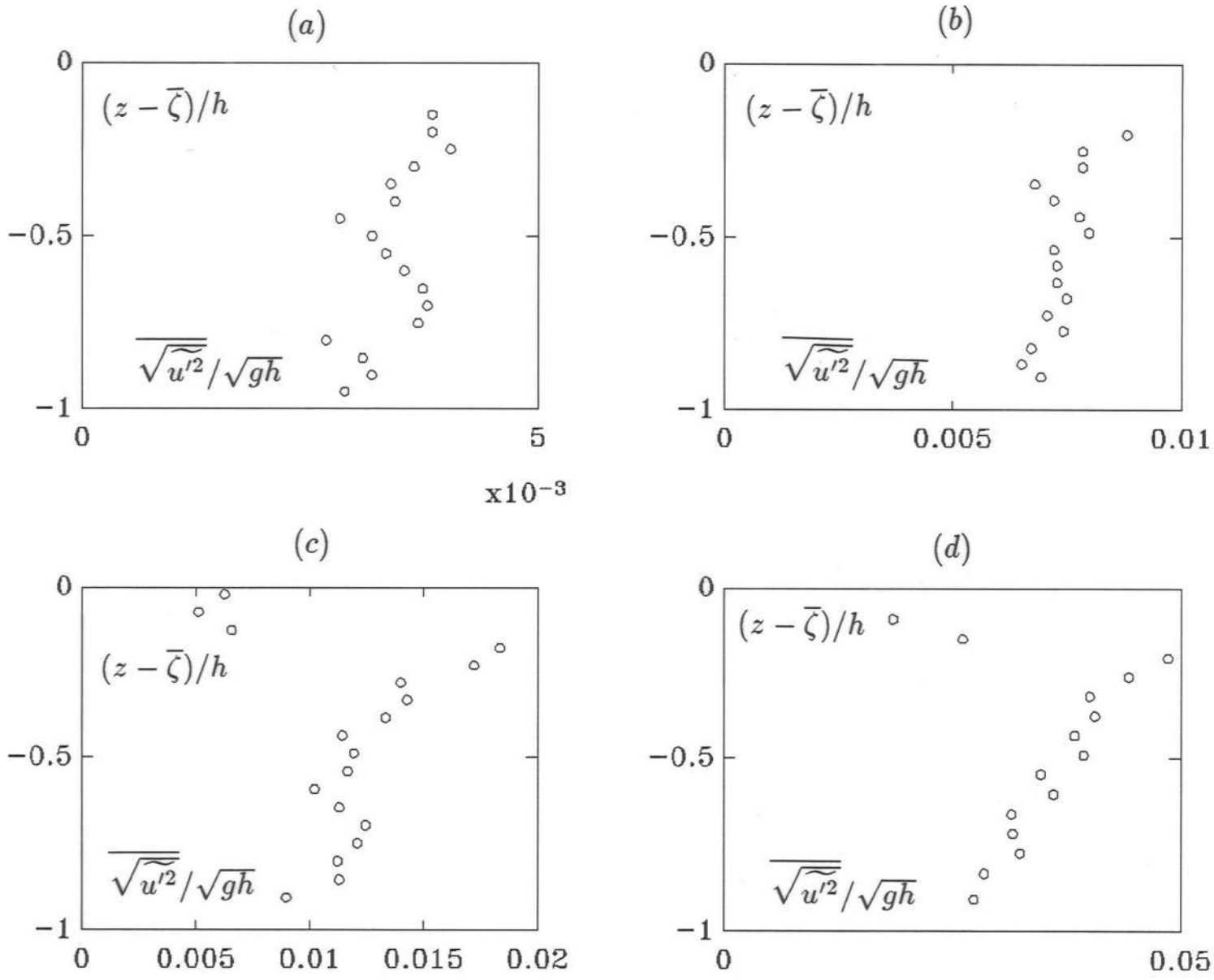
(a)
(b)
(c)
(d)
$(z-\overline{\zeta})/h$
$\overline{\sqrt{\widetilde{u'^2}}}/\sqrt{gh}$
0
−0.5
−1
0
5
x10^{-3}
0.005
0.01
0.015
0.02
0.05

FIGURE 6

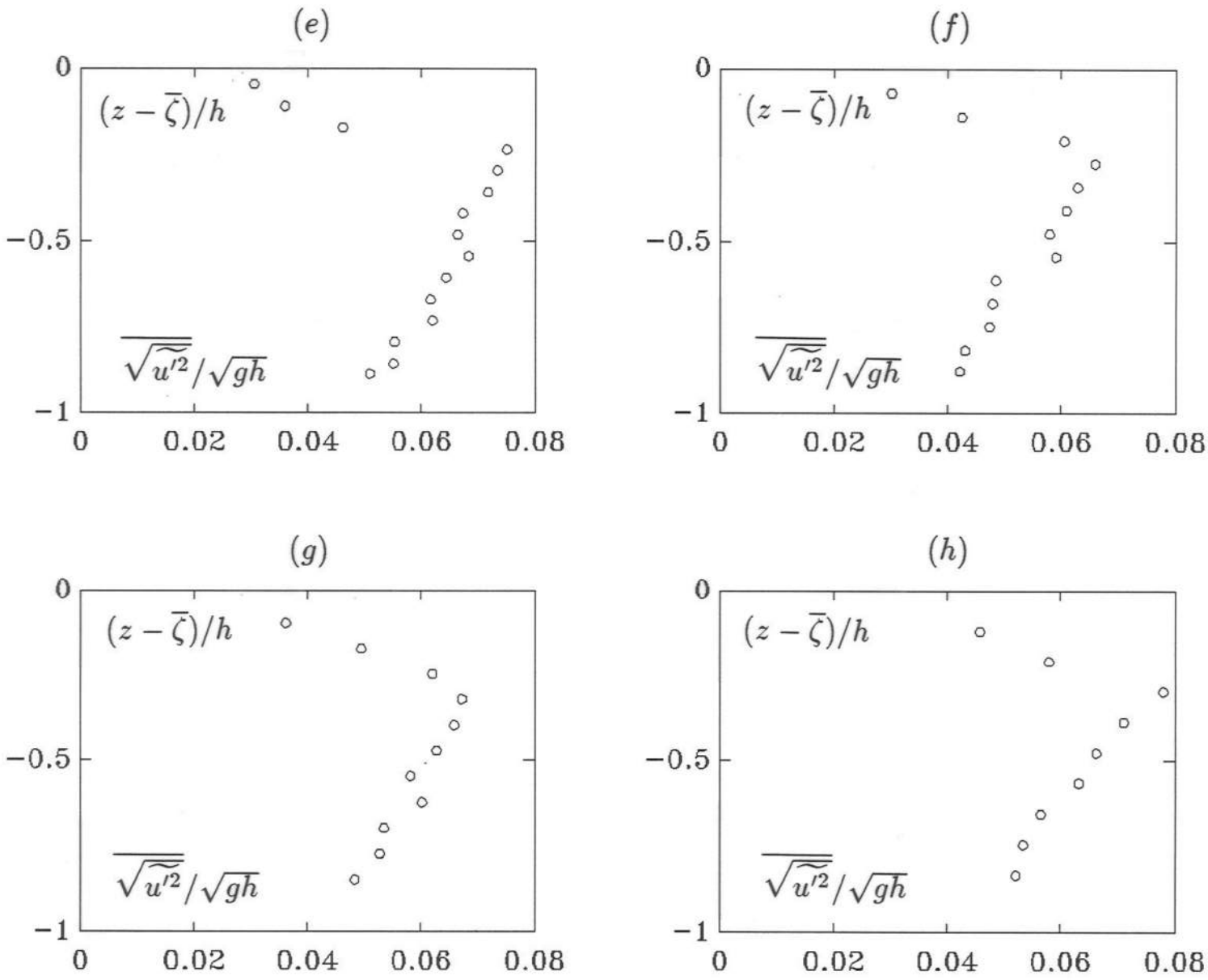

FIGURE 6 (Continued)

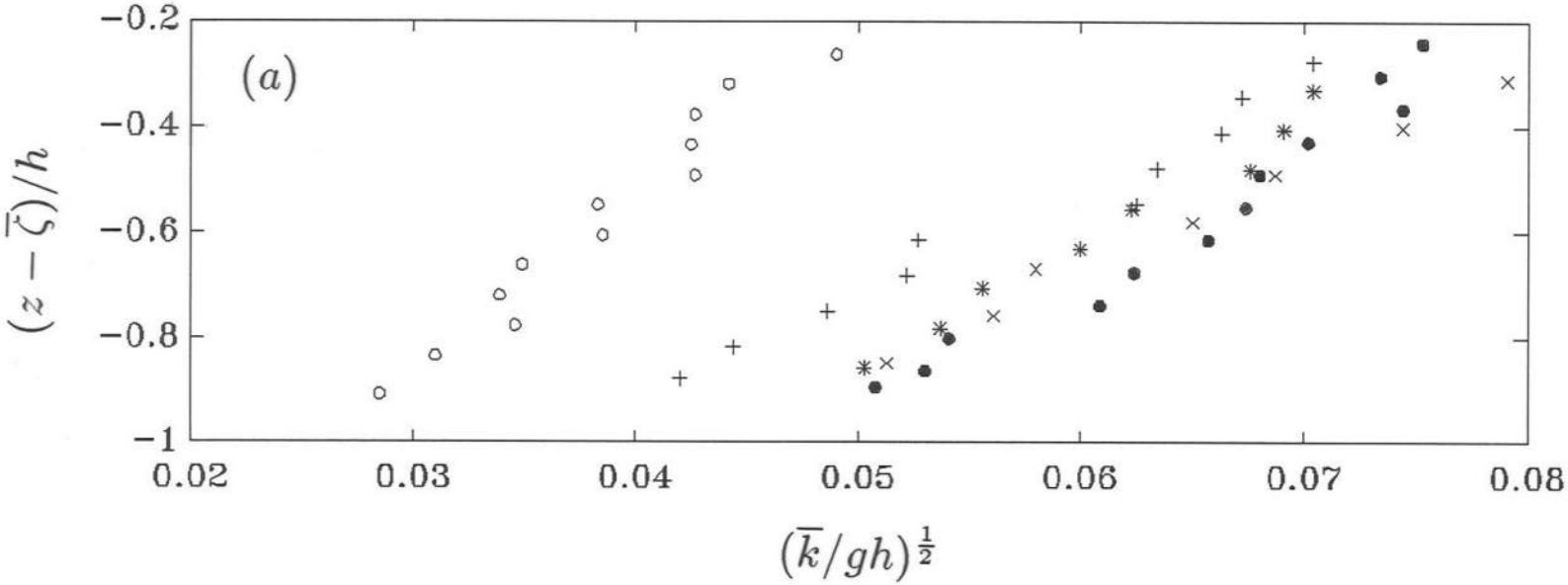
(a)
−0.2
−0.4
−0.6
−0.8
−1
0.02
0.03
0.04
0.05
0.06
0.07
0.08
$(z-\overline{\zeta})/h$
$(\overline{k}/gh)^{\frac{1}{2}}$

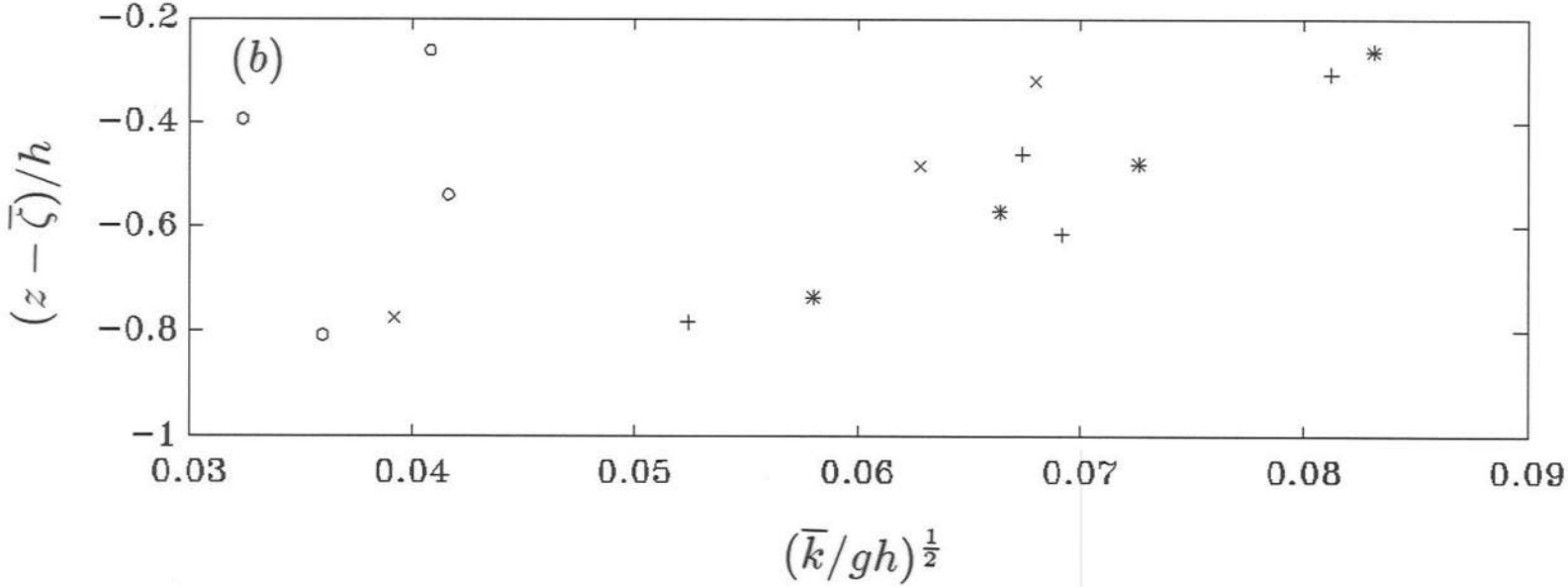
(b)
−0.2
−0.4
−0.6
−0.8
−1
0.03
0.04
0.05
0.06
0.07
0.08
0.09
$(z-\overline{\zeta})/h$
$(\overline{k}/gh)^{\frac{1}{2}}$

FIGURE 7

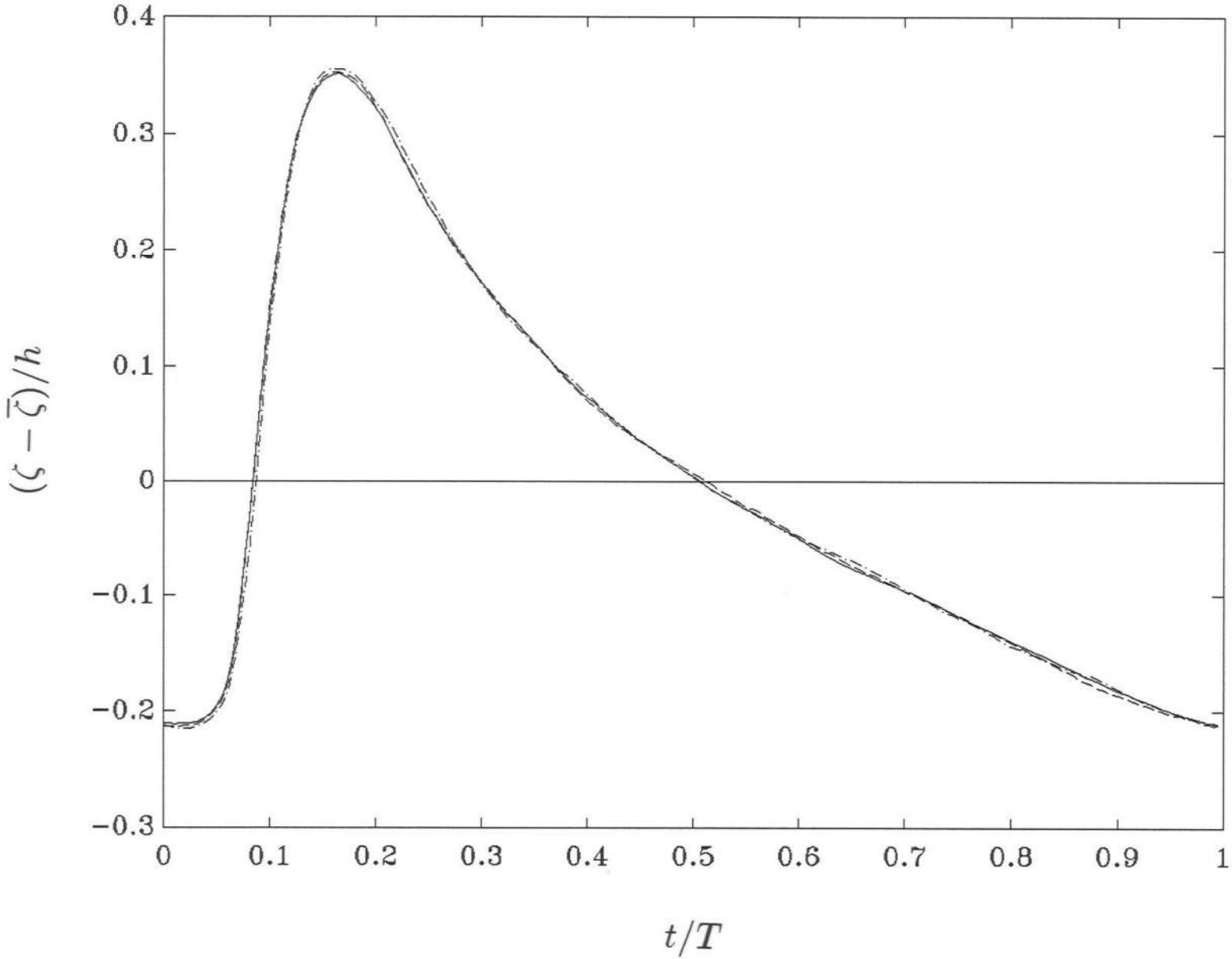

FIGURE 8

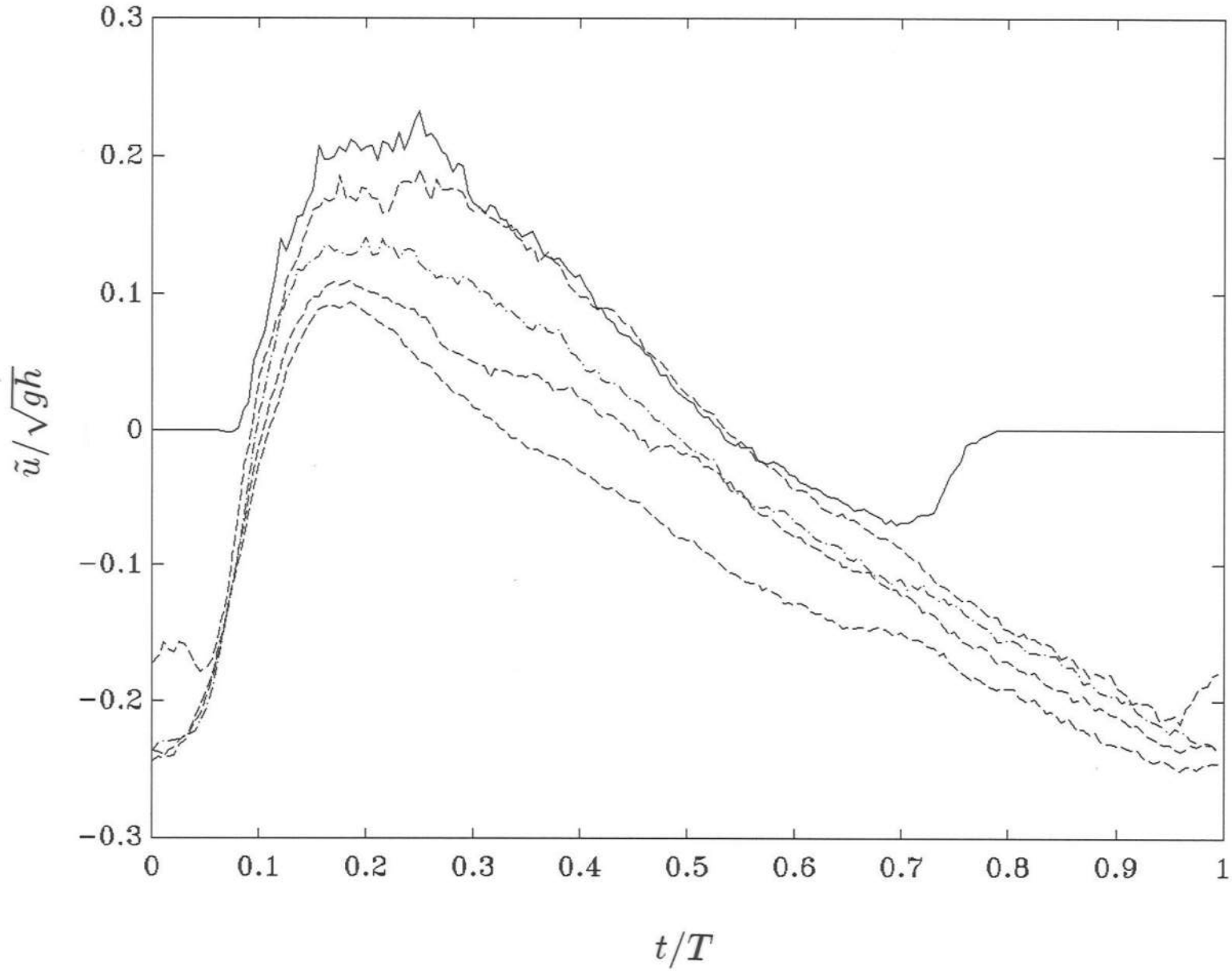

FIGURE 9

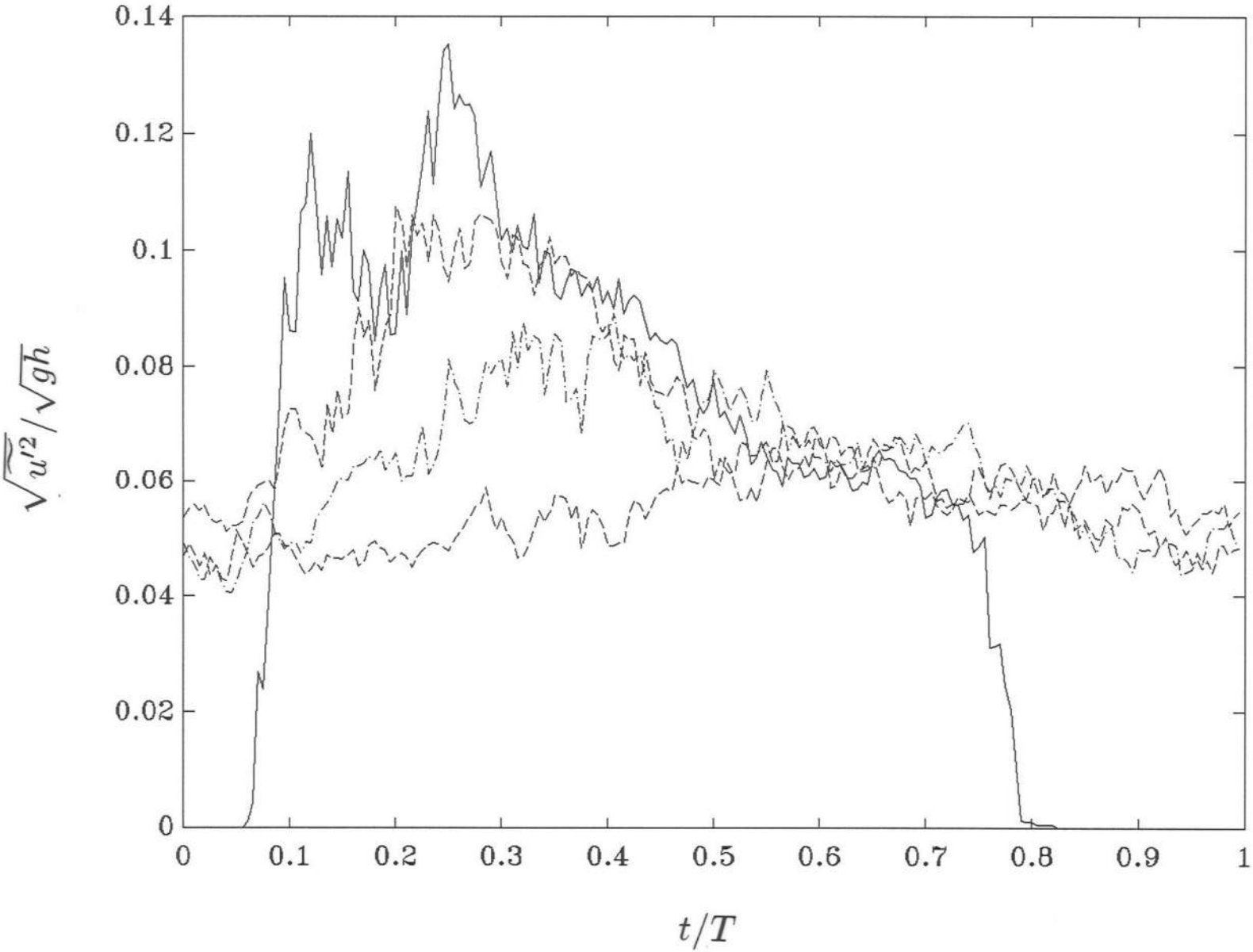
0.14
0.12
0.1
0.08
0.06
0.04
0.02
0
0
0.1
0.2
0.3
0.4
0.5
0.6
0.7
0.8
0.9
1
$\sqrt{\widetilde{u'^2}}/\sqrt{gh}$
t/T

FIGURE 10

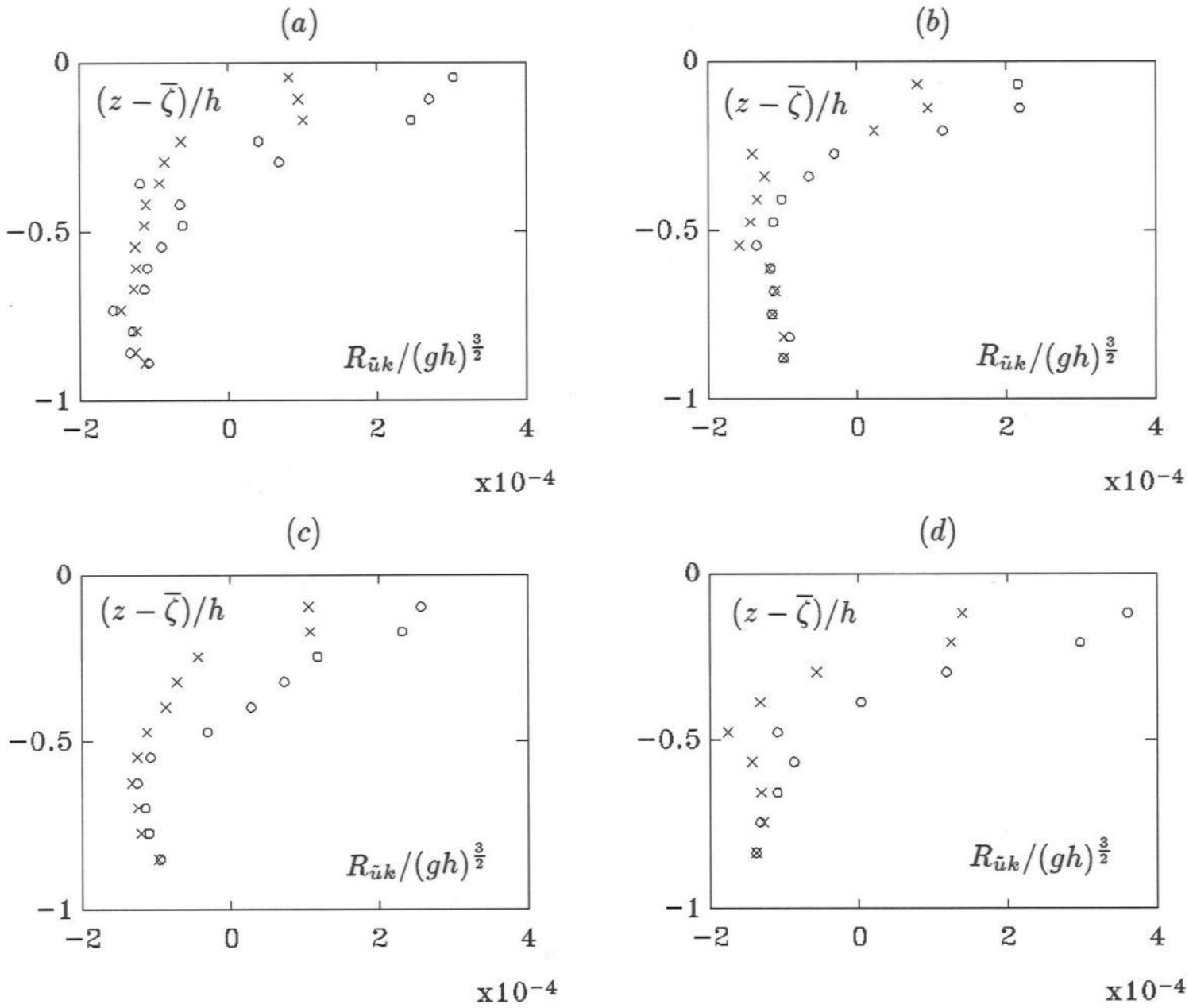

FIGURE 11

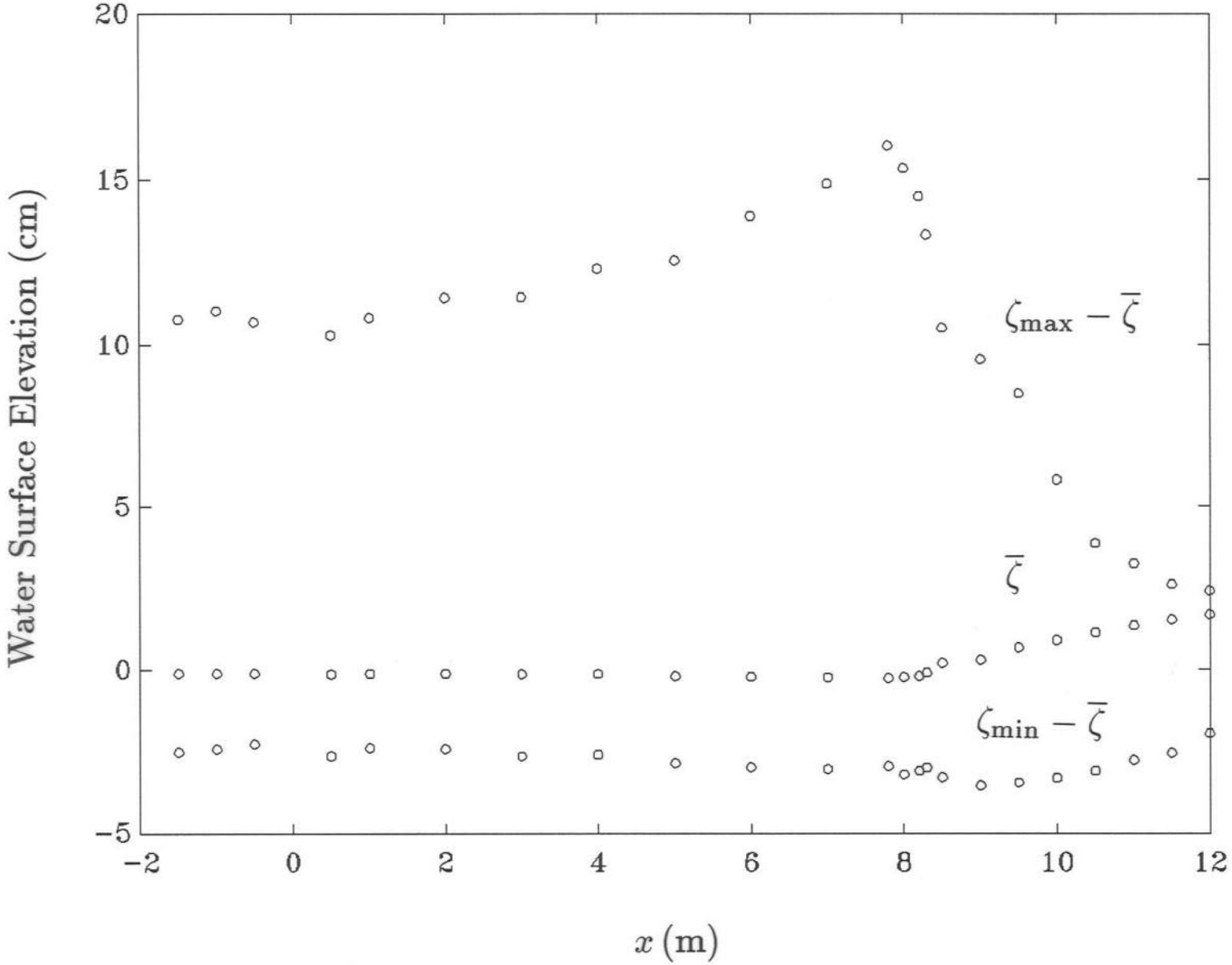
Water Surface Elevation (cm)
20
15
10
5
0
−5
−2
0
2
4
6
8
10
12
x (m)
$\zeta_{max} - \overline{\zeta}$
$\overline{\zeta}$
$\zeta_{min} - \overline{\zeta}$

FIGURE 12

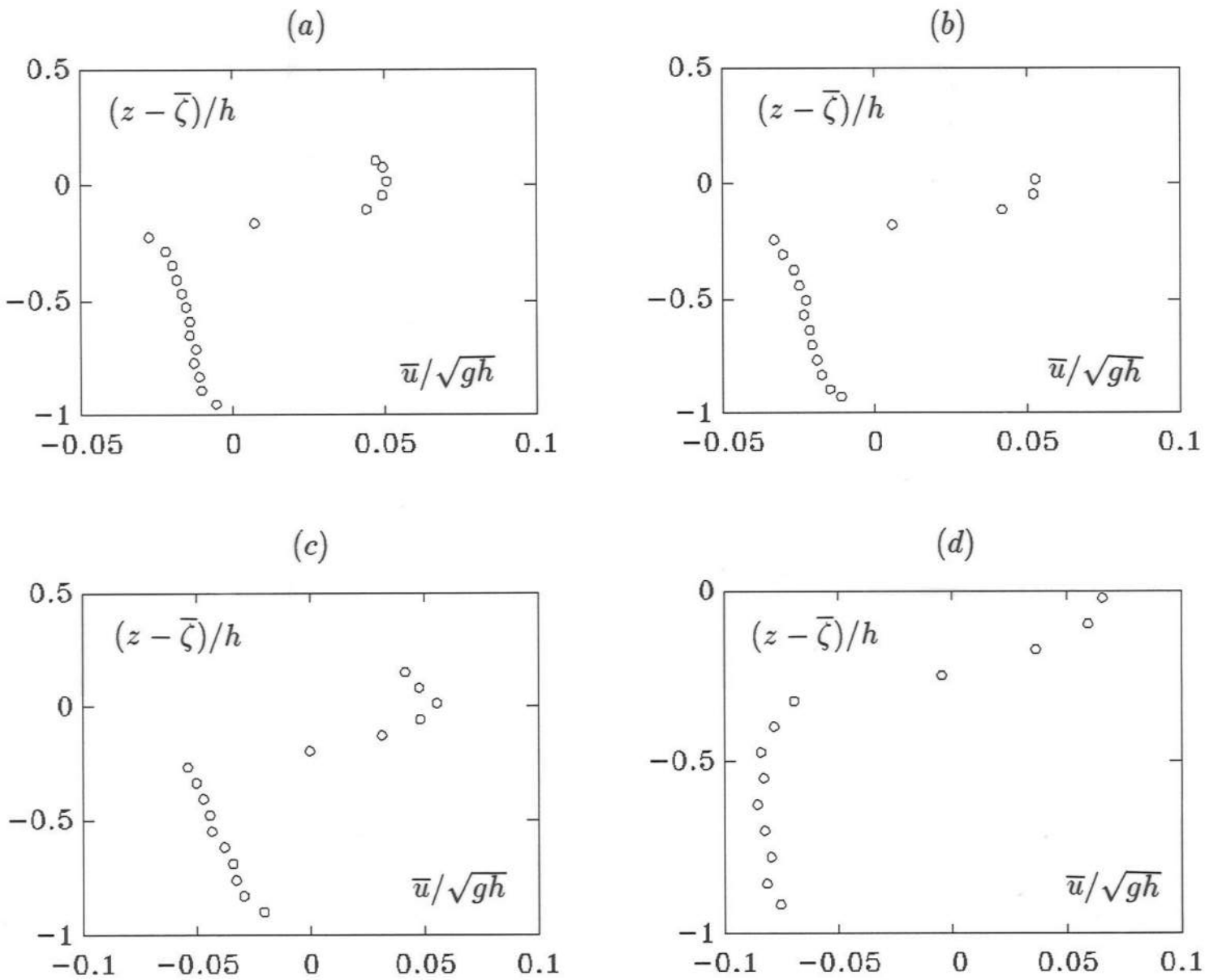
(a)
(b)
(c)
(d)
$(z-\overline{\zeta})/h$
$\overline{u}/\sqrt{gh}$
0.5
0
−0.5
−1
−0.1
−0.05
0
0.05
0.1

FIGURE 13

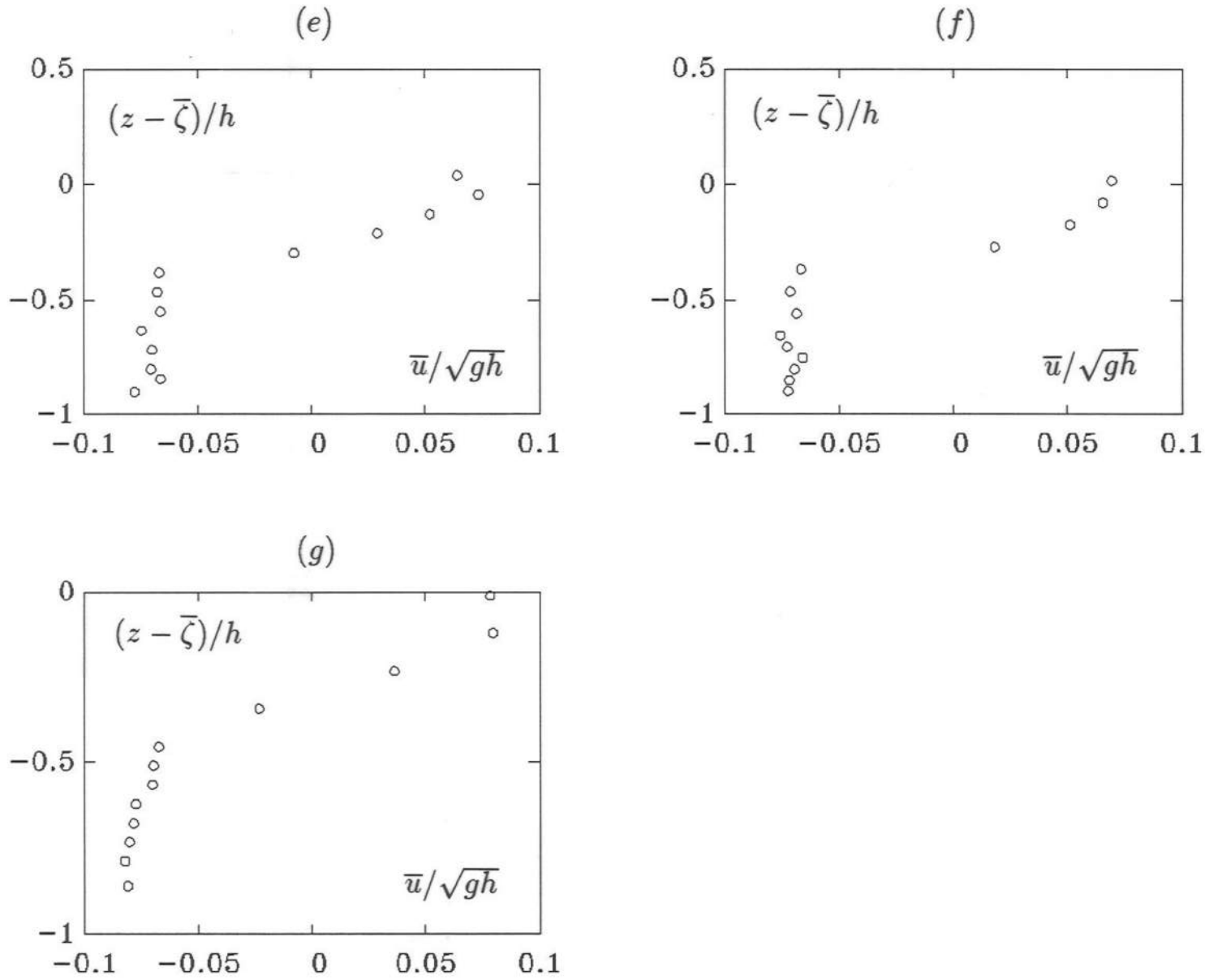

FIGURE 13 (Continued)

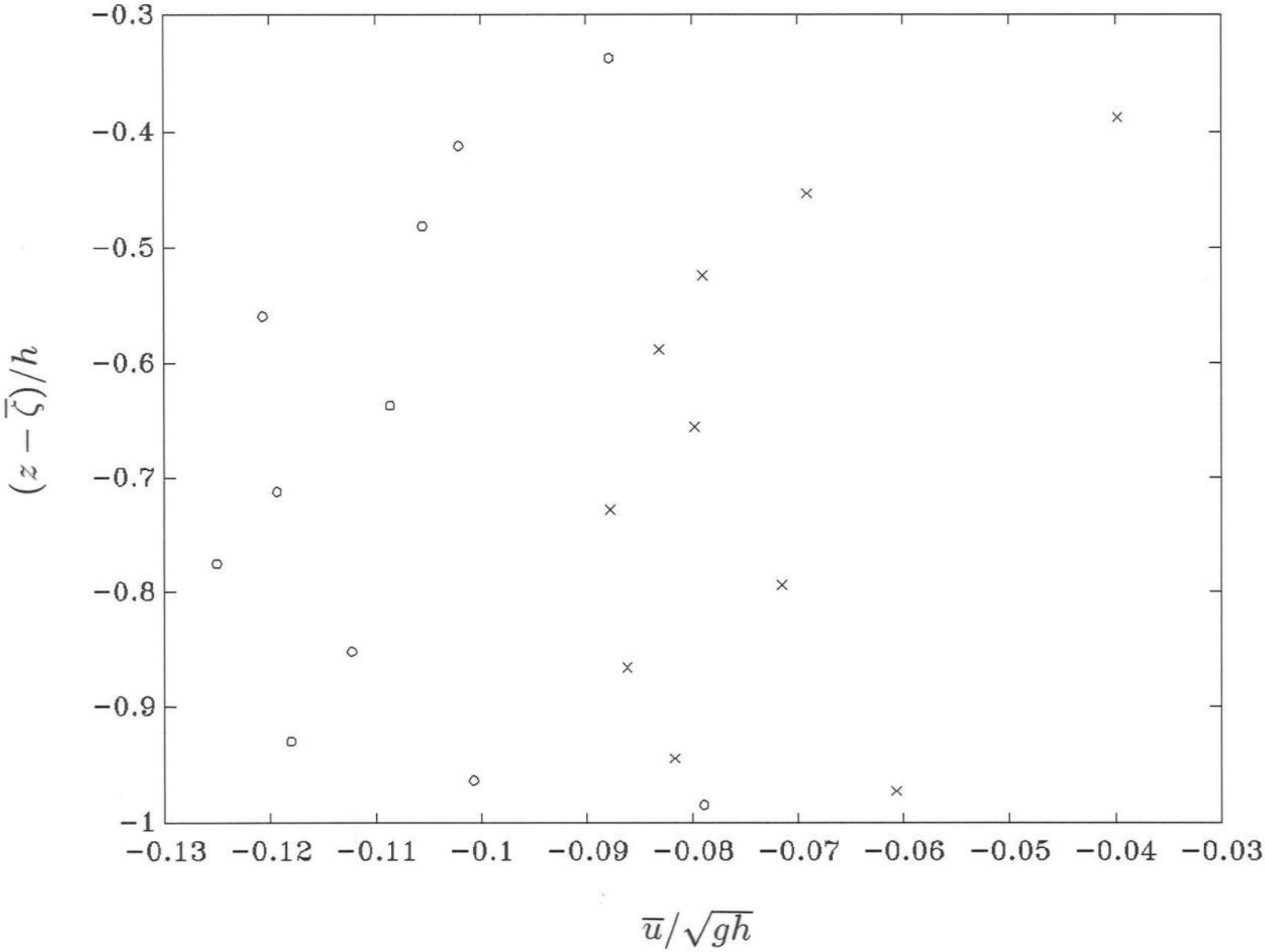
−0.3
−0.4
−0.5
−0.6
−0.7
−0.8
−0.9
−1
−0.13 −0.12 −0.11 −0.1 −0.09 −0.08 −0.07 −0.06 −0.05 −0.04 −0.03
$(z-\overline{\zeta})/h$
$\overline{u}/\sqrt{gh}$

FIGURE 14

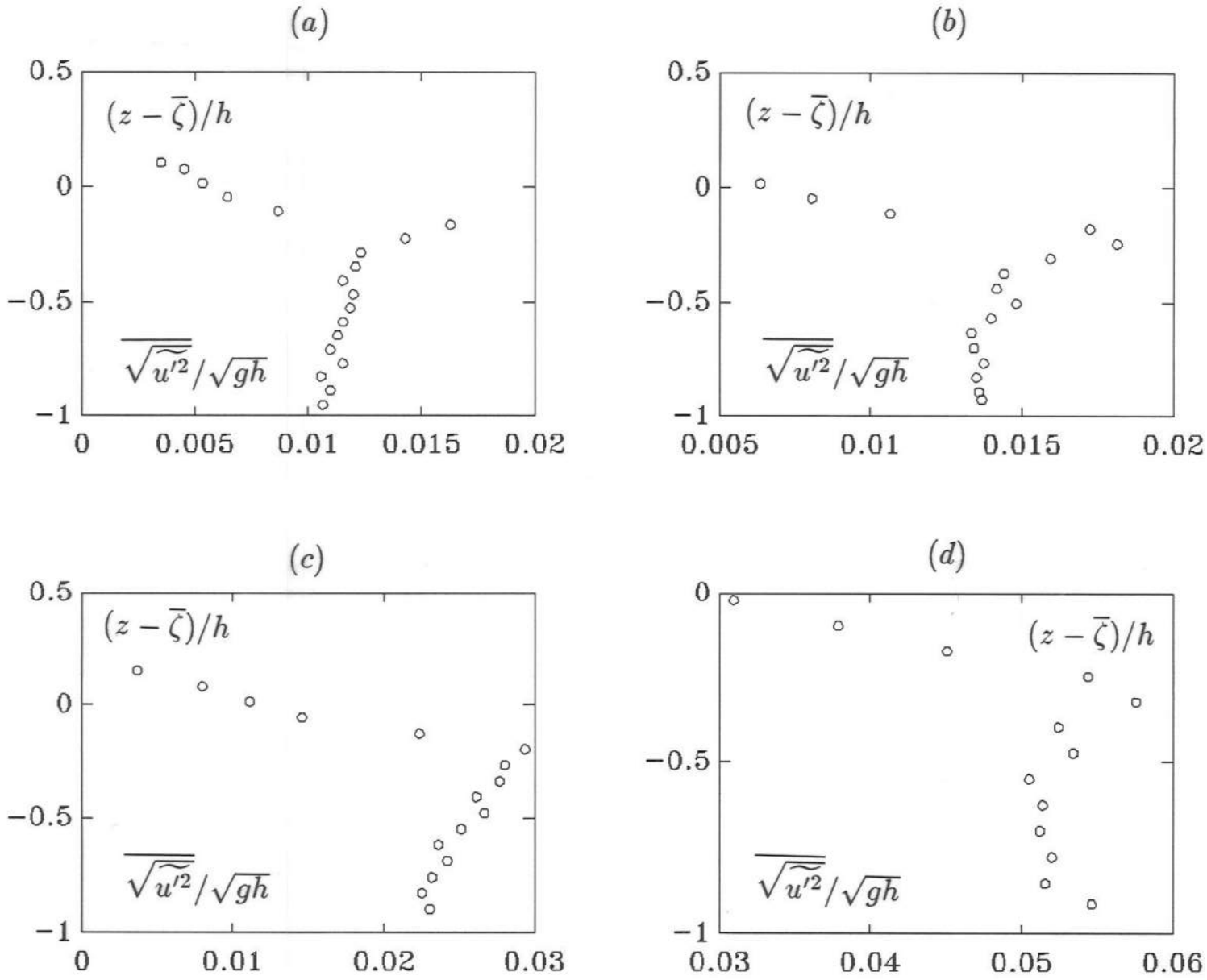
(a)
(b)
(c)
(d)
$(z-\overline{\zeta})/h$
$\overline{\sqrt{\widetilde{u'^2}}}/\sqrt{gh}$
0.5
0
−0.5
−1
0
0.005
0.01
0.015
0.02
0.03
0.04
0.05
0.06

FIGURE 15

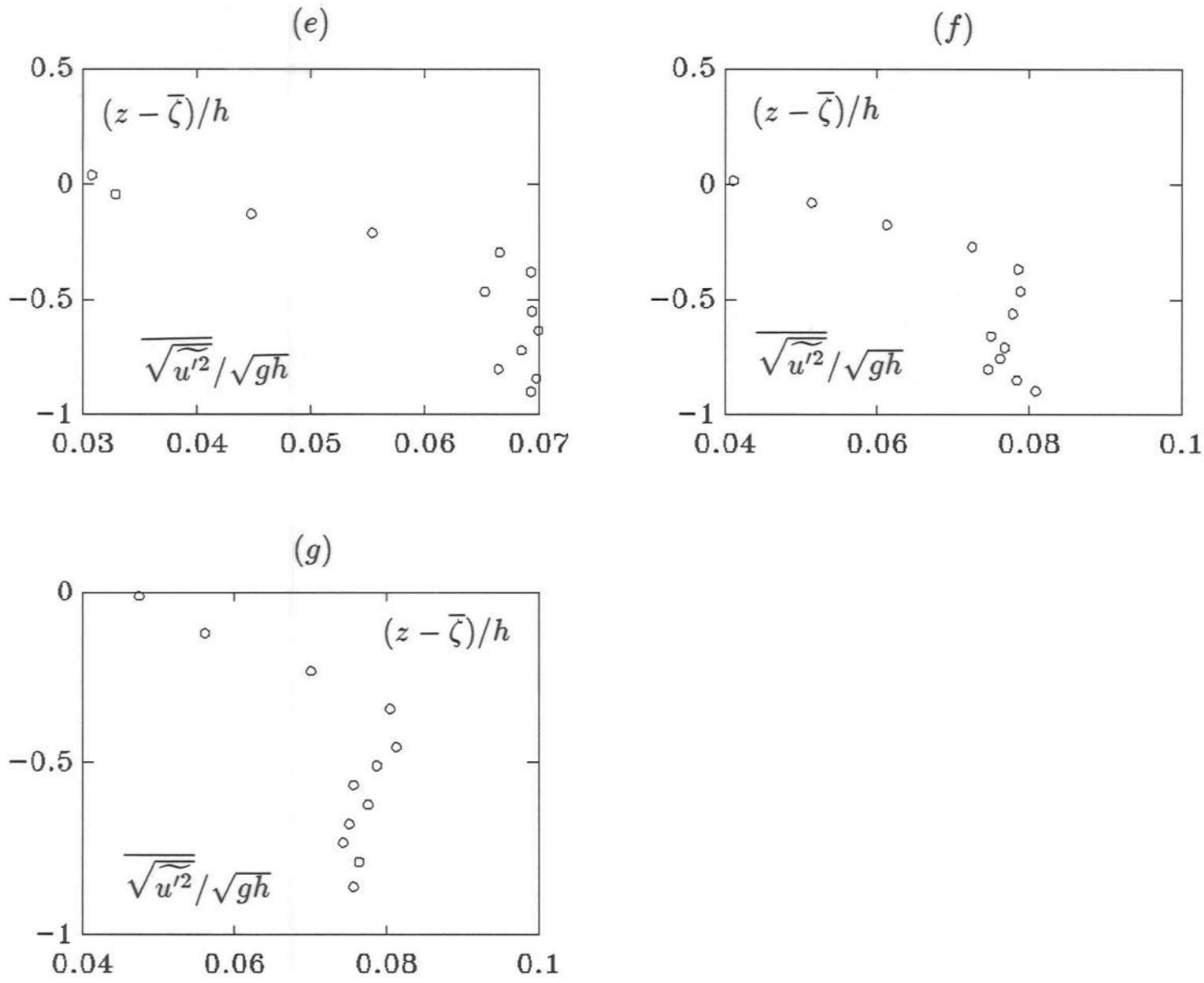

FIGURE 15 (Continued)

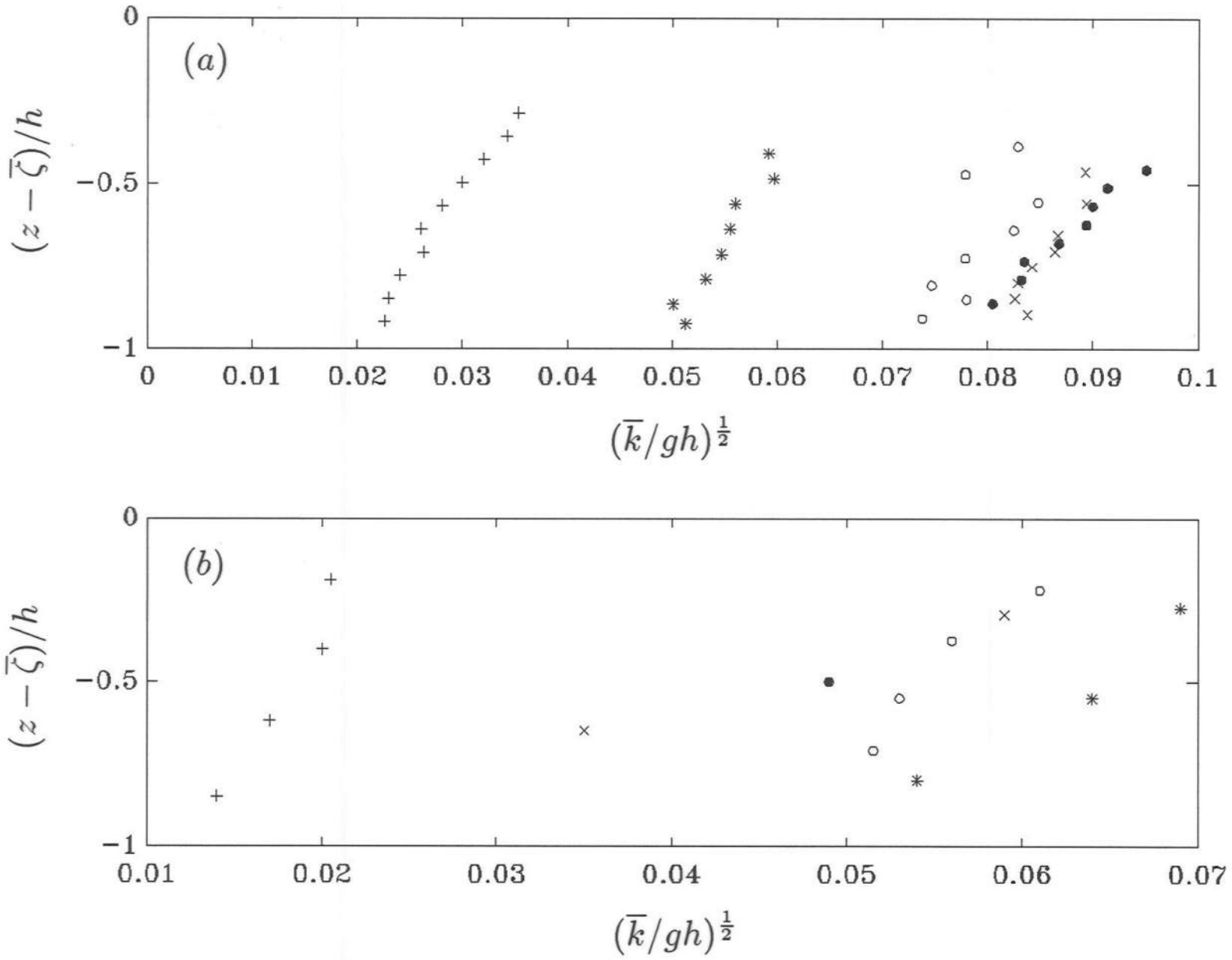
(a)
0
−0.5
−1
0
0.01
0.02
0.03
0.04
0.05
0.06
0.07
0.08
0.09
0.1
$(z-\overline{\zeta})/h$
$(\overline{k}/gh)^{\frac{1}{2}}$
(b)
0
−0.5
−1
0.01
0.02
0.03
0.04
0.05
0.06
0.07
$(z-\overline{\zeta})/h$
$(\overline{k}/gh)^{\frac{1}{2}}$

FIGURE 16

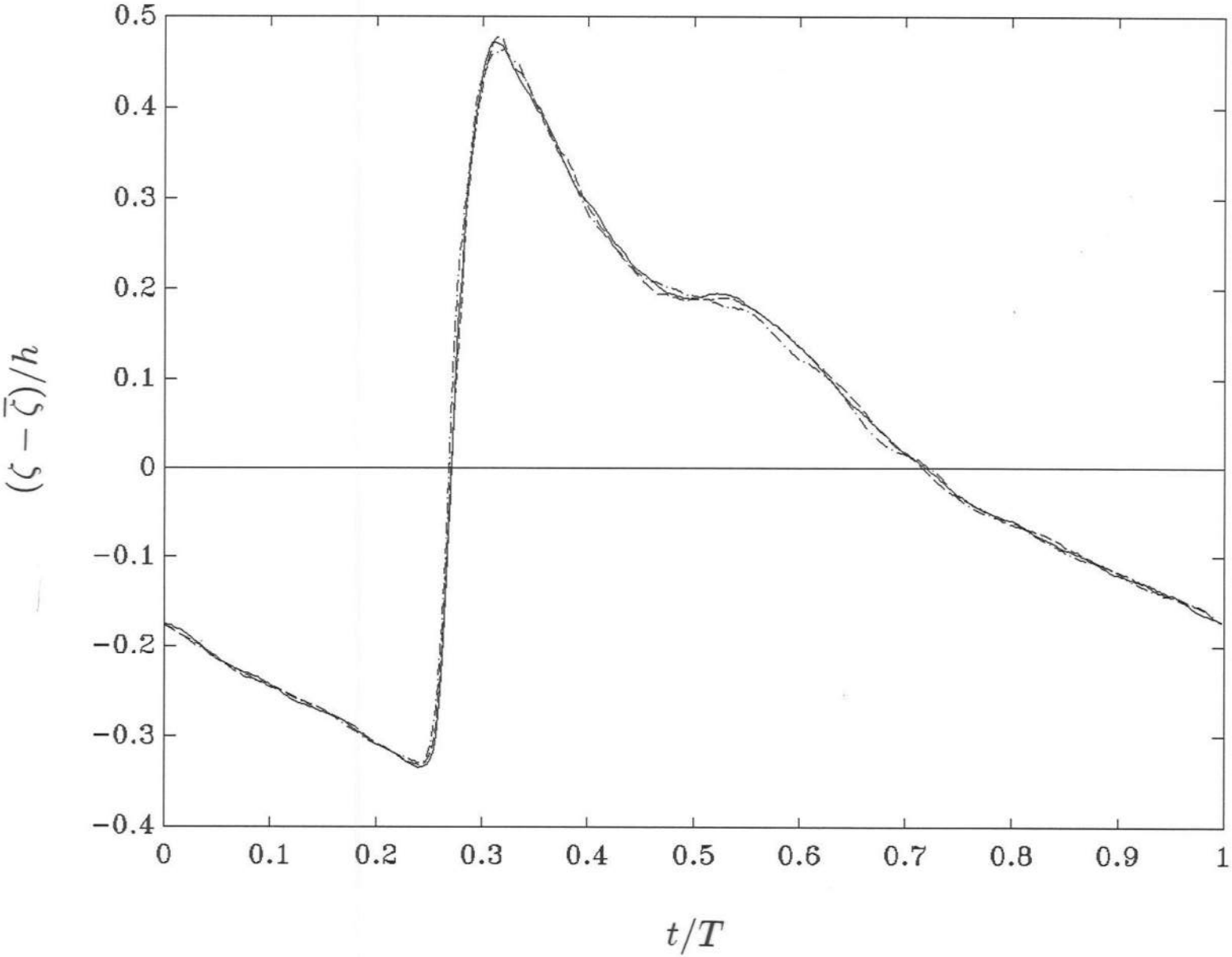
0.5
0.4
0.3
0.2
0.1
0
−0.1
−0.2
−0.3
−0.4
0
0.1
0.2
0.3
0.4
0.5
0.6
0.7
0.8
0.9
1
$(\zeta - \overline{\zeta})/h$
t/T

FIGURE 17

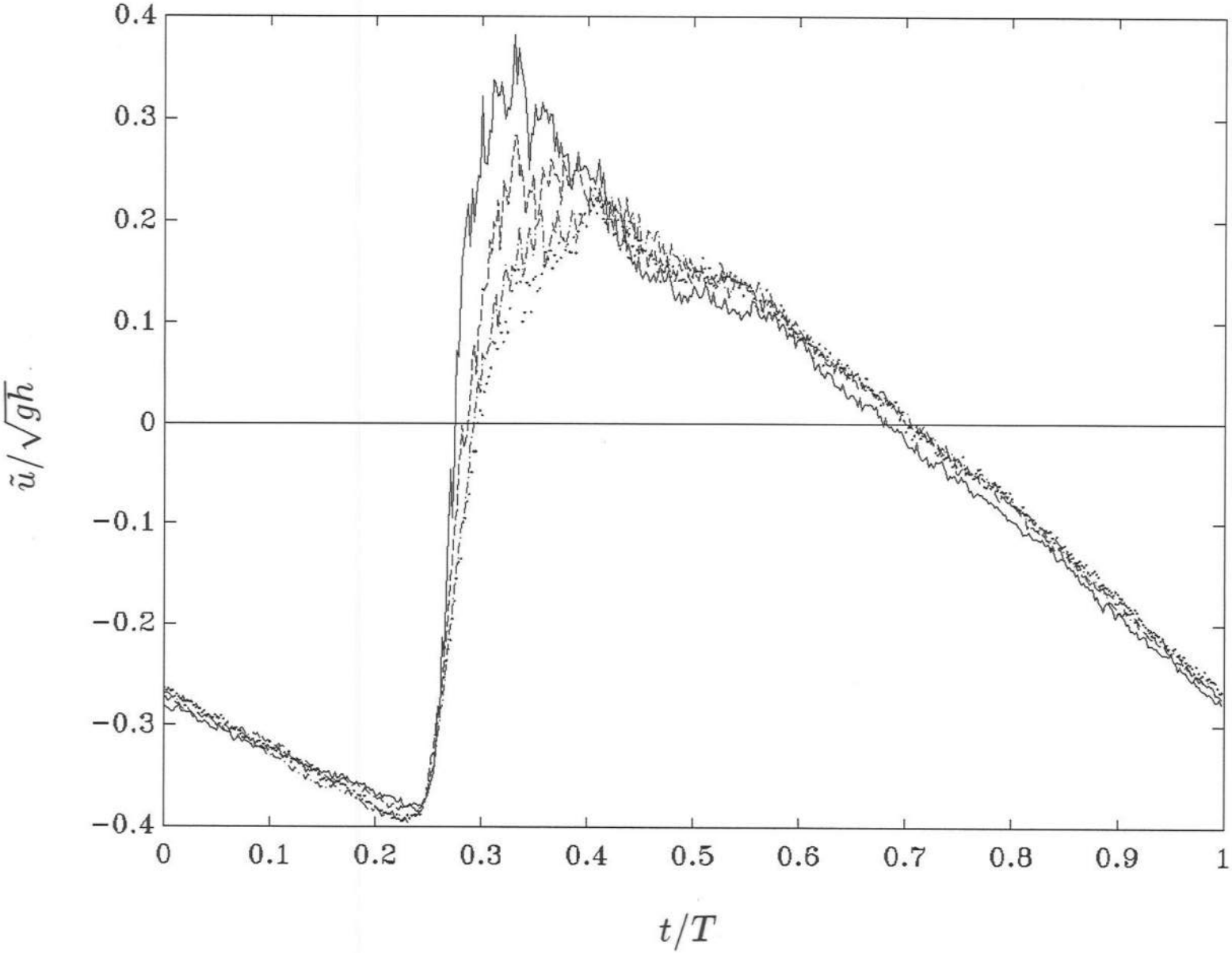
0.4
0.3
0.2
0.1
0
−0.1
−0.2
−0.3
−0.4
0
0.1
0.2
0.3
0.4
0.5
0.6
0.7
0.8
0.9
1
$\tilde{u}/\sqrt{gh}$
t/T

FIGURE 18

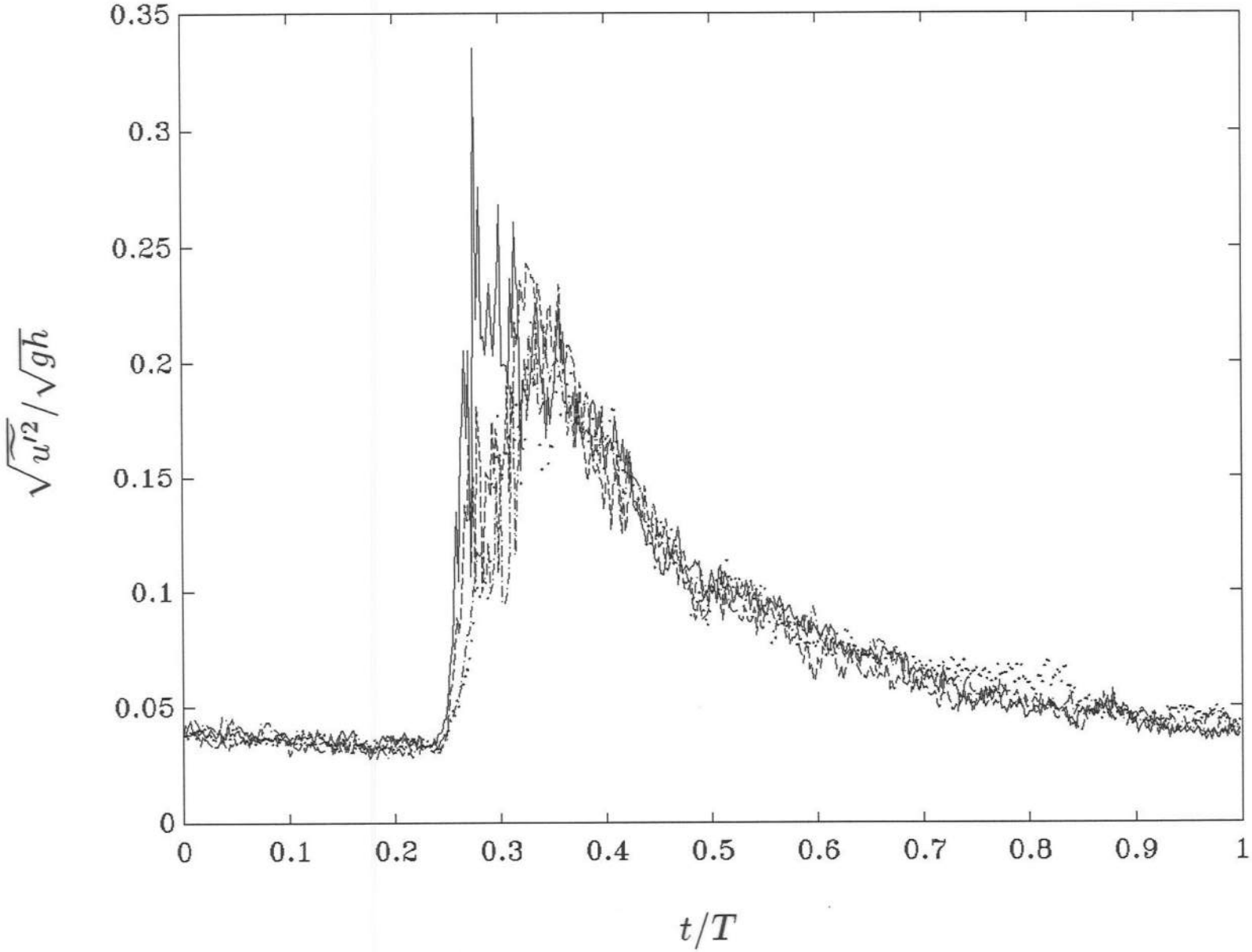
0.35
0.3
0.25
0.2
0.15
0.1
0.05
0
0
0.1
0.2
0.3
0.4
0.5
0.6
0.7
0.8
0.9
1
$\sqrt{\widetilde{u'^2}}/\sqrt{gh}$
t/T

FIGURE 19

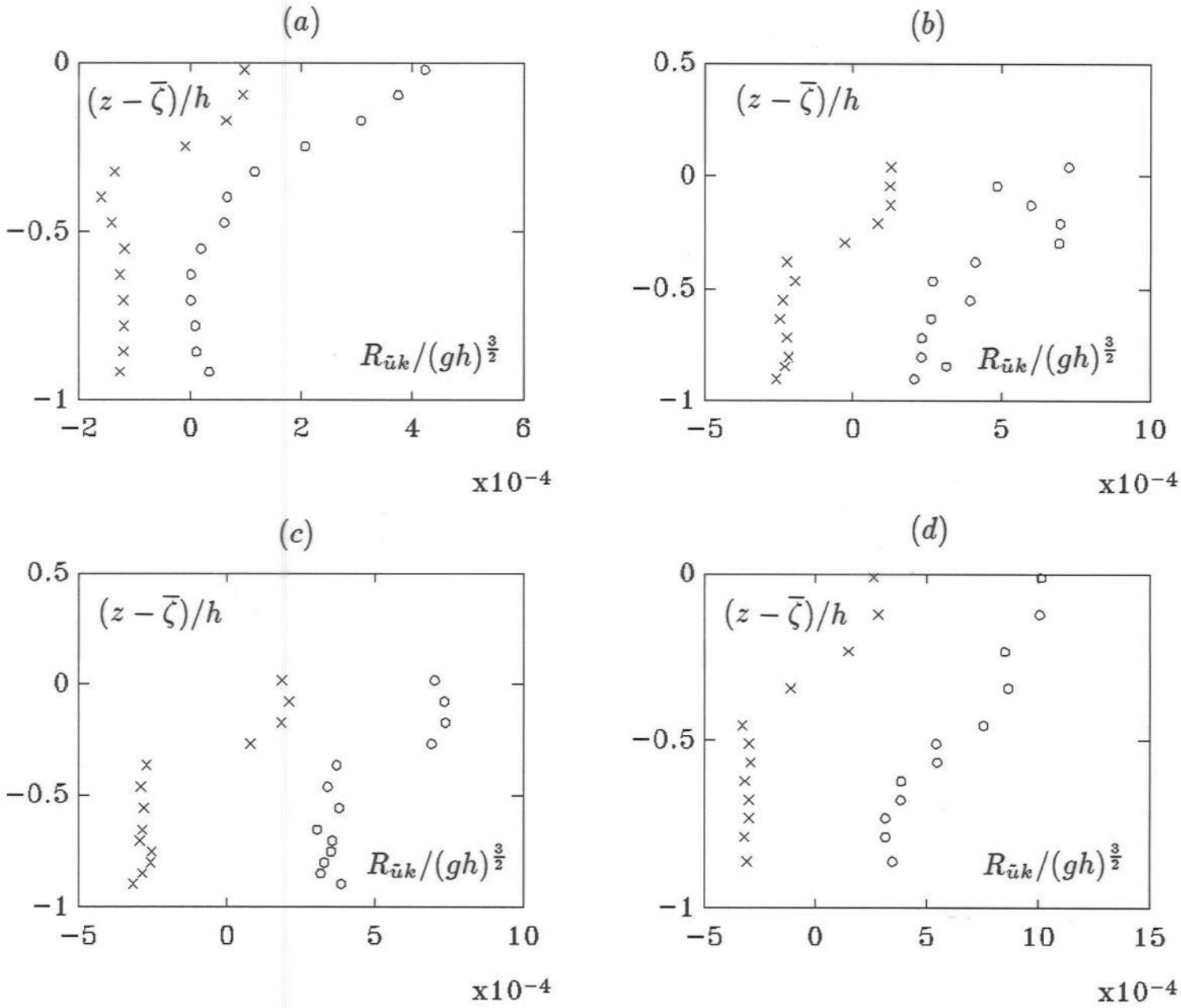

FIGURE 20